Shang *et al.*
Chinese Journal of Mechanical Engineering (2022) 35:53
https://doi.org/10.1186/s10033-022-00723-2

Chinese Journal of Mechanical Engineering

ORIGINAL ARTICLE

Open Access

Rotation Angle Control Strategy for Telescopic Flexible Manipulator Based on a Combination of Fuzzy Adjustment and RBF Neural Network

Dongyang Shang[1], Xiaopeng Li[1*], Meng Yin[2], Fanjie Li[1] and Bangchun Wen[1]

Abstract

The length of flexible manipulators with a telescopic arm alters during movement. The dynamic parameters of telescopic flexible manipulators exhibit significant time-varying characteristics owing to variations in length. With an increase in the manipulators' length, the nonlinear terms caused by flexibility in the manipulators' dynamic equations cannot be ignored. The time-varying characteristics and nonlinear terms of telescopic flexible manipulators cause fluctuations in rotation angles, which affect the operation accuracy of end-effectors. In this study, a control strategy based on a combination of fuzzy adjustment and an RBF neural network is utilized to improve the control accuracy of flexible telescopic manipulators. First, the dynamic equation of the manipulators is established using the assumed mode method and Lagrange's principle, and the influence of nonlinear terms is analyzed. Subsequently, a combined control strategy is proposed to suppress the fluctuation of the rotation angle in telescopic flexible manipulators. The variation ranges of the feedforward PD controller parameters are determined by the pole placement strategy and length of the manipulators. Fuzzy rules are utilized to adjust the controller parameters in real-time. The RBF neural network is utilized to identify and compensate the uncertain part of the dynamic model of the flexible manipulators. The uncertain part comprises time-varying parameters and nonlinear terms. Finally, numerical simulations and prototype experiments prove the effectiveness of the combined control strategy. The results prove that the proposed control strategy has a smaller standard deviation of errors. Therefore, the combined control strategy is more suitable for telescopic flexible manipulators, which can effectively improve the control accuracy of rotation angles.

Keywords: Flexible manipulator, RBF neural network, Fuzzy control, Dynamic uncertainty

1 Introduction

A flexible manipulator with a telescopic arm alters its arm's length through movement of the telescopic arm. Telescopic flexible manipulators are more conducive for grasping objects. Flexible manipulators are widely utilized in several fields such as space exploration [1], intelligent assembly, warehousing, and logistics. In Ref. [2], a telescopic flexible manipulator with navigation capabilities is installed on a vehicle to realize the automatic grasping of objects. In Refs. [3, 4], a flexible manipulator is placed on a wheeled vehicle. Thus, a novel mobile platform with flexible manipulators is proposed. A flexible manipulator with variable structure is proposed in Ref. [5]. Telescopic flexible manipulators have a larger radius of rotation and lighter mass. The deformation of the flexible manipulator is more significant at the end of the manipulator. During movement, vibrations are more likely to occur because of flexibility. The vibration of flexible manipulators significantly affects the movement

*Correspondence: xpli@me.neu.edu.cn

[1] School of Mechanical Engineering and Automation, Northeastern University, Shenyang 110819, China
Full list of author information is available at the end of the article

accuracy of end-effectors and causes the robot's task to fail. In addition, because of flexibility, it is more difficult to control the rotation angles of the flexible manipulators. Therefore, researches on the control of flexible manipulators have an important engineering significance.

The establishment of precise dynamic equations is a prerequisite for the control of flexible manipulators. The dynamic methods of flexible manipulators mainly include the assumed mode method (AMM) and finite element (FE) method. The AMM considers that the lateral deformation of flexible manipulators is a two-dimensional function of the time and mode. In Ref. [6], the AMM is utilized to establish the dynamic equation of flexible manipulators. In Ref. [7], the influence of the mass at the end of flexible manipulators is considered in the modeling processes. In Ref. [8], dynamic equations of flexible manipulators with two-dimensional (transverse and longitudinal) deformations are established. In Ref. [9], the dynamic model of the rigid-flexible coupling manipulator is established using the AMM. However, it is impossible to obtain an accurate dynamic model for manipulators with complex structures using the AMM. Refs. [10, 11] employ the FE method and Lagrange principle to establish a dynamic model of flexible manipulators. In Ref. [12], the FE method is employed to establish the dynamic model of flexible manipulators with flexible joints. In Ref. [13], the FE method is established as a dynamic model of flexible telescopic manipulators. The dynamic equations of the flexible manipulator established by AMM and FE method contain the nonlinear factors of rigid-flexible coupling which cause the vibration of flexible manipulators.

The length of the manipulator alters during the movement of a telescopic flexible manipulator. The change in the manipulator's length causes time variations in the dynamic parameters. In addition, nonlinear terms are coupled with rigid and flexible terms in the dynamic equations of flexible manipulators. The time-varying characteristics of the dynamic parameters and nonlinear terms constitute an uncertain part of the flexible-manipulator model. This uncertainty increases the difficulty when controlling flexible manipulators. For the control research of manipulators, the main intelligent control strategies, such as robust control strategy [14, 15], sliding mode control strategy [16, 17], backstepping control strategy [18], and fuzzy control (FC) strategy [19, 20] have been adopted. In Ref. [14], a robust controller with a linear quadratic Gaussian is designed to control the rotation angle of flexible manipulators. An adaptive sliding mode control strategy is employed to control the flexible manipulator in Ref. [21]. In Refs. [22, 23], the stability of the backstepping control strategy is proved by the Lyapunov theorem. In Ref. [24], fuzzy rules are adopted to adjust the parameters of a proportional-integral-differential (PID) controller, thereby improving the motion accuracy of anthropomorphic manipulators. In Ref. [25], the FC is applied to control manipulators, and a control method combining a sliding mode control strategy is proposed. With the continuous development of neural networks, Refs. [26, 27] apply neural networks to control the dynamics of flexible manipulators. In Ref. [28], neural networks are utilized to identify the uncertain part in the manipulator dynamics model. In addition, the uncertain part after identification is compensated by the control law in the form of feedback. Therefore, neural networks can be utilized to identify the uncertain parts of flexible manipulators, thereby improving the control accuracy.

According to Ref. [29], a telescopic flexible manipulator can be equivalent to a flexible beam model with variable length. This study employs AMM and Lagrange's principles to establish the dynamic equations of flexible manipulators. The influence of nonlinear terms on the deformation of flexible manipulators is discussed. The combined control strategy of fuzzy adjustment and RBF neural network is used to control the rotation angle of the flexible manipulators. The uncertainty component of the flexible manipulator model comprises time-varying dynamic parameters and flexible coupling nonlinear terms. The uncertain part is identified by the RBF neural network and re-compensated in the control system. This can effectively improve the accuracy of the input torque of the flexible manipulators and achieve accurate control. The main contribution of this study is the use of pole placement strategy and the flexible manipulator length to determine the range of the controller parameters. The parameters of the controller are adjusted in real time using fuzzy rules. The RBF neural network is utilized to identify and compensate for the uncertainty of the flexible manipulator model, and fuzzy rules are used to improve the control accuracy.

The rest of this paper is organized as follows: In Section 2, the dynamic equations of flexible manipulators are established using AMM and Lagrange's principle. In addition, the influence of the flexible-coupling nonlinear terms is analyzed. In Section 3, the combined control strategy based on the fuzzy adjustment and RBF neural network is employed to control the flexible manipulator servo system, and the stability of the system is proved using the Lyapunov theorem. In Section 4, a numerical simulation and physical control experiment of the

flexible manipulator's servo system are presented. Finally, Section 5 presents the conclusions of this study.

2 Influence of Flexible Coupling Nonlinear Terms

A telescopic flexible manipulator comprises non-retractable and telescopic arms, as illustrated in Figure 1. The telescopic flexible manipulator rotates horizontally. The telescopic arm creates an axially translating movement along with a fixed manipulator. The vibration phenomenon occurs when the telescopic flexible manipulator rotates under the action of the driving torque. Vibration affects the movement accuracy of the end-effectors. According to Ref. [13], the telescopic flexible manipulator is equivalent to a flexible beam model with a variable length.

In Figure 1, $w(x,t)$ denotes the deformation of flexible manipulators, which is a two-dimensional function of position x and time t; T_a denotes the input torque of flexible manipulators; θ denotes the rotation angle of flexible manipulators; XOY denotes the static coordinate system, and x_0Oy_0 denotes the dynamic coordinate system.

2.1 Kinetic Energy and Potential Energy of Flexible Manipulator

$$\begin{cases} r^{\mathrm{T}} = [X, Y], \\ X = x\cos\theta - w(x,t)\sin\theta, \\ Y = x\sin\theta + w(x,t)\cos\theta, \\ w(x,t) = \sum_{i=1}^{\infty} \phi_i(x)\delta_i(t), \end{cases} \tag{1}$$

where $\phi_i(x)$ denotes the modal function, and $\delta_i(t)$ denotes the modal coordinate.

The kinetic energy of flexible manipulators is expressed as

$$T = \frac{1}{2}\rho A \int_0^l \dot{r}^{\mathrm{T}}\dot{r}\,\mathrm{d}x, \tag{2}$$

where ρ denotes the volume density of flexible manipulators, and A denotes the cross-sectional area of the flexible manipulators.

The potential energy of flexible manipulators is expressed as

$$V = \frac{1}{2}EI \int_0^l \left(\frac{\partial^2 w(x,t)}{\partial x^2}\right)^2 \mathrm{d}x, \tag{3}$$

where EI denotes the flexural rigidity of flexible manipulators.

According to Eqs. (2) and (3), the kinetic energy of flexible manipulators is not only related to the rotation angle, but also closely related to the deformation. The value of the modal function is closely related to boundary conditions. According to Refs. [28, 30], the expression for the modal function can be obtained as

$$\begin{cases} \phi_i(x) = \mathrm{ch}\beta_i x - \cos\beta_i x + \varsigma_i(\mathrm{sh}\beta_i x - \sin\beta_i x), \\ \varsigma_i = -\dfrac{\mathrm{sh}\beta_i l - \sin\beta_i l}{\mathrm{ch}\beta_i l + \cos\beta_i l}, \\ \cos\beta_i l \mathrm{ch}\beta_i l = -1, \end{cases} \tag{4}$$

where l denotes the length of the flexible manipulators, and β_i denotes the characteristic root of the modal function, which is closely related to the modal frequency of the flexible manipulators. The expression of β_i can be expressed as

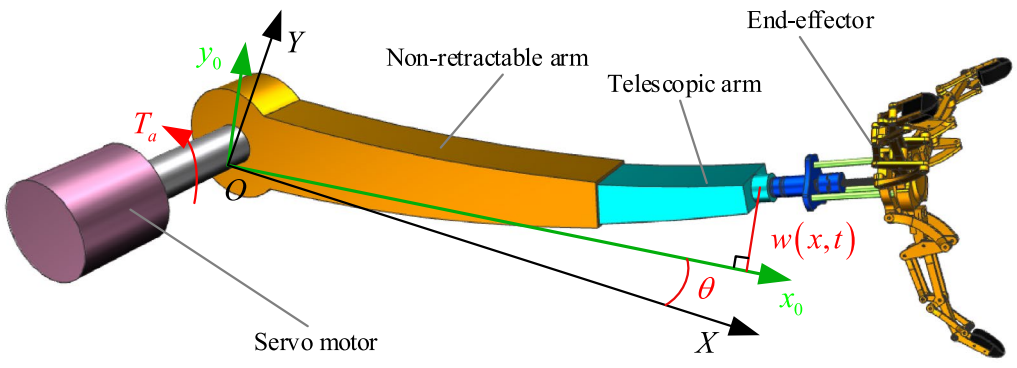

Figure 1 Schematic diagram of the telescopic flexible manipulator

$$\beta_i^4 = \frac{\omega_i^2 \rho A}{EI}, \tag{5}$$

where ω_i denotes the modal frequency of flexible manipulators.

2.2 Dynamic Model of Flexible Manipulator

Regardless of the external force required for the movement of the telescopic arm, Eq. (6) can be obtained using the Lagrange dynamic equation.

$$\frac{\mathrm{d}}{\mathrm{d}t}\left(\frac{\partial T}{\partial \dot{q}_i}\right) - \frac{\partial T}{\partial q_i} + \frac{\partial V}{\partial q_i} = Q_i, \tag{6}$$

where q_1 denotes the rotation angle of the flexible manipulators; q_2 denotes the ith mode coordinate of the flexible manipulators, and Q_i denotes the generalized force.

Eq (6) is expressed as:

$$\begin{cases} \dfrac{\mathrm{d}}{\mathrm{d}t}\left(\dfrac{\partial T}{\partial \dot{\theta}}\right) - \dfrac{\partial T}{\partial \theta} + \dfrac{\partial V}{\partial \theta} = T_a, \\ \dfrac{\mathrm{d}}{\mathrm{d}t}\left(\dfrac{\partial T}{\partial \dot{\delta}_i(t)}\right) - \dfrac{\partial T}{\partial \delta_i(t)} + \dfrac{\partial V}{\partial \delta_i(t)} = 0. \end{cases} \tag{7}$$

After sorting, Eq. (8) can be obtained.

$$\begin{cases} T_a = \ddot{\theta}\displaystyle\int_0^l \rho A x^2 \mathrm{d}x + \ddot{\theta}\sum_{i=1}^{\infty}\delta_i(t)^2 + 2\dot{\theta}\sum_{i=1}^{\infty}\delta_i(t)\dot{\delta}_i(t) + \sum_{i=1}^{\infty}\ddot{\delta}_i(t)\int_0^l \rho A x\phi_i(x)\mathrm{d}x, \\ \displaystyle\sum_{i=1}^{\infty}\ddot{\delta}_i(t) + \ddot{\theta}\sum_{i=1}^{\infty}\int_0^l \rho A x\phi_i(x)\mathrm{d}x - \dot{\theta}^2\sum_{i=1}^{\infty}\delta_i(t) + \sum_{i=1}^{\infty}\omega_i^2\delta_i(t) = 0. \end{cases} \tag{8}$$

According to Eq. (8), the dynamic equation of flexible manipulators can be expressed as follows:

$$\begin{cases} I_a\ddot{\theta} + \ddot{\theta}\displaystyle\sum_{i=1}^{\infty}\delta_i(t)^2 + 2\dot{\theta}\sum_{i=1}^{\infty}\delta_i(t)\dot{\delta}_i(t) + \sum_{i=1}^{\infty}\ddot{\delta}_i(t)F_{ai} = T_a, \\ \displaystyle\sum_{i=1}^{\infty}\ddot{\delta}_i(t) + \ddot{\theta}\sum_{i=1}^{\infty}F_{ai} - \dot{\theta}^2\sum_{i=1}^{\infty}\delta_i(t) + \sum_{i=1}^{\infty}\omega_i^2\delta_i(t) = 0, \\ I_a = \rho A\displaystyle\int_0^l x^2\mathrm{d}x, \\ F_{ai} = \displaystyle\int_0^l \rho A x\phi_i(x)\mathrm{d}x. \end{cases} \tag{9}$$

After removing the nonlinear terms coupling the rotation angle and modal coordinates, the following can be obtained:

$$\begin{cases} I_a\ddot{\theta} + \displaystyle\sum_{i=1}^{\infty}\ddot{\delta}_i(t)F_{ai} = T_a, \\ \displaystyle\sum_{i=1}^{\infty}\ddot{\delta}_i(t) + \ddot{\theta}\sum_{i=1}^{\infty}F_{ai} + \sum_{i=1}^{\infty}\omega_i^2\delta_i(t) = 0. \end{cases} \tag{10}$$

Equation (10) represents the dynamic equation of the flexible manipulators moving in the horizontal plane.

2.3 Influence of Nonlinear Terms

A simulation calculation of the deformation of flexible manipulators is proposed to study the influence of nonlinear terms on the dynamic model. The single-link calculation proposed by Damaren [31] is adopted as a function of the rotation angle and time, and expressed as follows:

$$\ddot{\theta}(t) = \begin{cases} \dfrac{\dot{\theta}_{\max}}{15}\left(1 - \cos\dfrac{2\pi}{15}(t)\right) & 0 \le t \le 15\,, \\ 0 & 15 \le t. \end{cases} \tag{11}$$

The maximum speed of the rotation angle can be set to 6 rad/s and 3 rad/s to characterize high-speed and low-speed movements, respectively.

Parameters such as the length and flexural rigidity of flexible manipulators affect deformation. When only the first-order model is considered, the deformation of the flexible manipulators can be obtained using Eqs. (9) and (10), as illustrated in Figures 2 and 3. In the analysis, it is assumed that the mass of the flexible manipulators remains unchanged. This assumption is based on the fact that the mass of telescopic flexible manipulators does not change during movement. Figure 2 illustrates the deformation and deformation deviation of flexible manipulators at a high speed. Figure 3 illustrates the deformation and deformation deviations of the flexible manipulators at low speed. In this study, the ratio of the flexible manipulator's deformation to the manipulator's length is used to characterize the deformability.

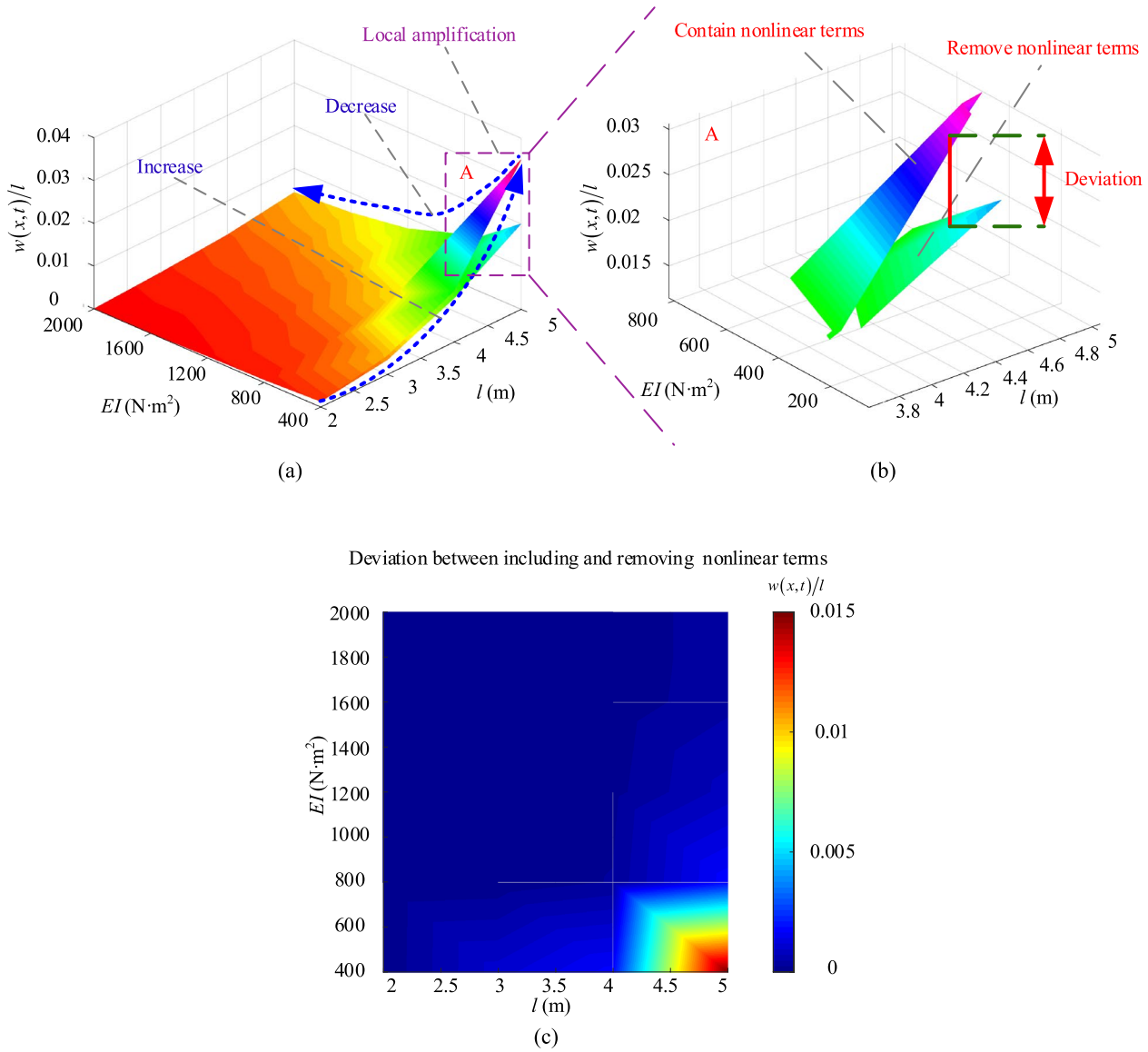

Figure 2 Deformation of flexible manipulators at high speed: (**a**) Relationship between deformability and length as well as flexural rigidity, (**b**) Partial enlarged view of (**a**), (**c**) Influence of nonlinear terms on deformation

The arrow represents the relationship between the deformability, length, and flexural rigidity of flexible manipulators.

According to Figures 2 and 3, the following conclusions can be drawn as follows.

1. The deformation of flexible manipulators increases rapidly with an increase in the manipulator's length. Deformability increases as the length of the manipulators increase. The deformation of the flexible manipulators decreases with an increase in flexural rigidity. Deformability decreases as the flexural rigidity of the manipulators increase. The same conclusion can be obtained for both the high-speed and low-speed movement states.
2. The deformation of the flexible manipulators is more significant under high-speed movement. The main reason for this is that a higher input torque is required for high-speed movement. The increase

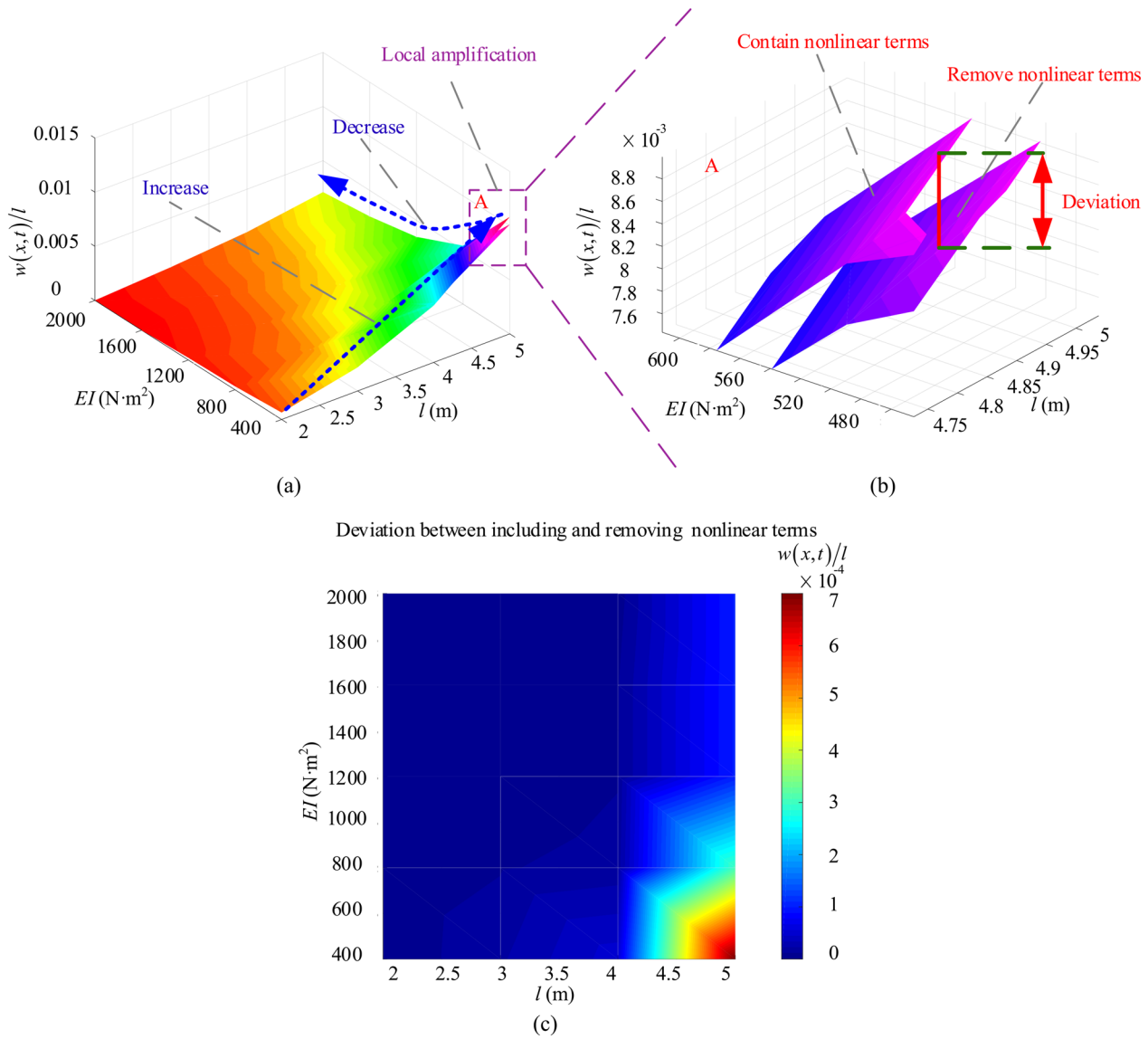

Figure 3 Deformation of flexible manipulators at low speed: (**a**) Relationship between deformability and length as well as flexural rigidity, (**b**) Partial enlarged view of (**a**), (**c**) Influence of nonlinear terms on deformation

in the input torque makes the deformation of the flexible manipulators more obvious.

3. Whether the nonlinear terms are considered or ignored, the same conclusion can be drawn. The deformation of flexible manipulators increases with an increase in the manipulators' length and a decrease in the flexural rigidity.
4. The deviation caused by ignoring the nonlinear terms increases rapidly with an increase in the manipulator length. The deviation gradually decreases with an increase in the flexural rigidity. The same conclusion can be obtained for both the high-speed and low-speed movement states.
5. The deviation caused by ignoring the nonlinear terms can be ignored in the state of low-speed movement, but cannot be ignored in the state of high-speed movement and long length of flexible manipulators.

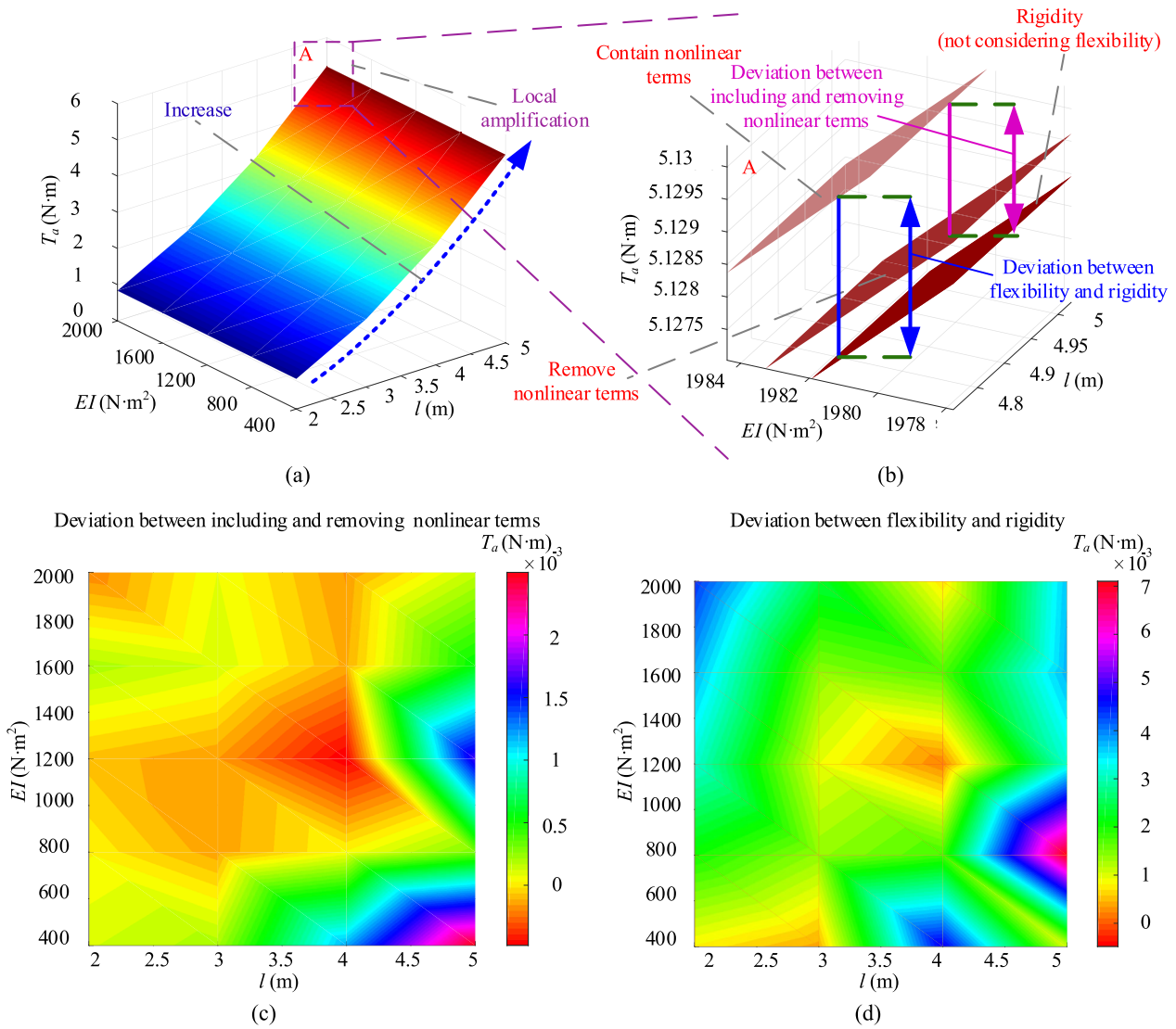

Figure 4 Input torque of flexible manipulators at high speed: (**a**) Relationship between input torque, length and flexural rigidity, (**b**) Partial enlarged view of (**a**), (**c**) Influence of nonlinear terms on input torque, (**d**) Influence of flexibility on input torque

In summary, according to the above conclusions, when the flexible manipulators are long and in a state of high-speed movement, the deviation caused by the nonlinear terms cannot be ignored. However, the deviation caused by the nonlinear terms can be ignored under other conditions.

To study the influence of the nonlinear terms on the input torque of flexible manipulators, the input torque is calculated according to Eqs. (9) and (10). When the first-order mode is solely considered, parameters such as manipulator's length and flexural rigidity affect the deformation of flexible manipulators. The influence rules are illustrated in Figures 4 and 5. The motor type is selected based on the maximum input torque. Therefore, the input torque in Figures 4 and 5 is the maximum input torque during the movement of flexible manipulators. Figure 4 illustrates the input torque and input torque's deviation of the flexible manipulators at high speed. Figure 5 illustrates the input torque and input torque's deviation of the flexible manipulators at low speed. The arrow indicates the relationship between the input torque of the flexible manipulators, manipulators' length, and flexural rigidity.

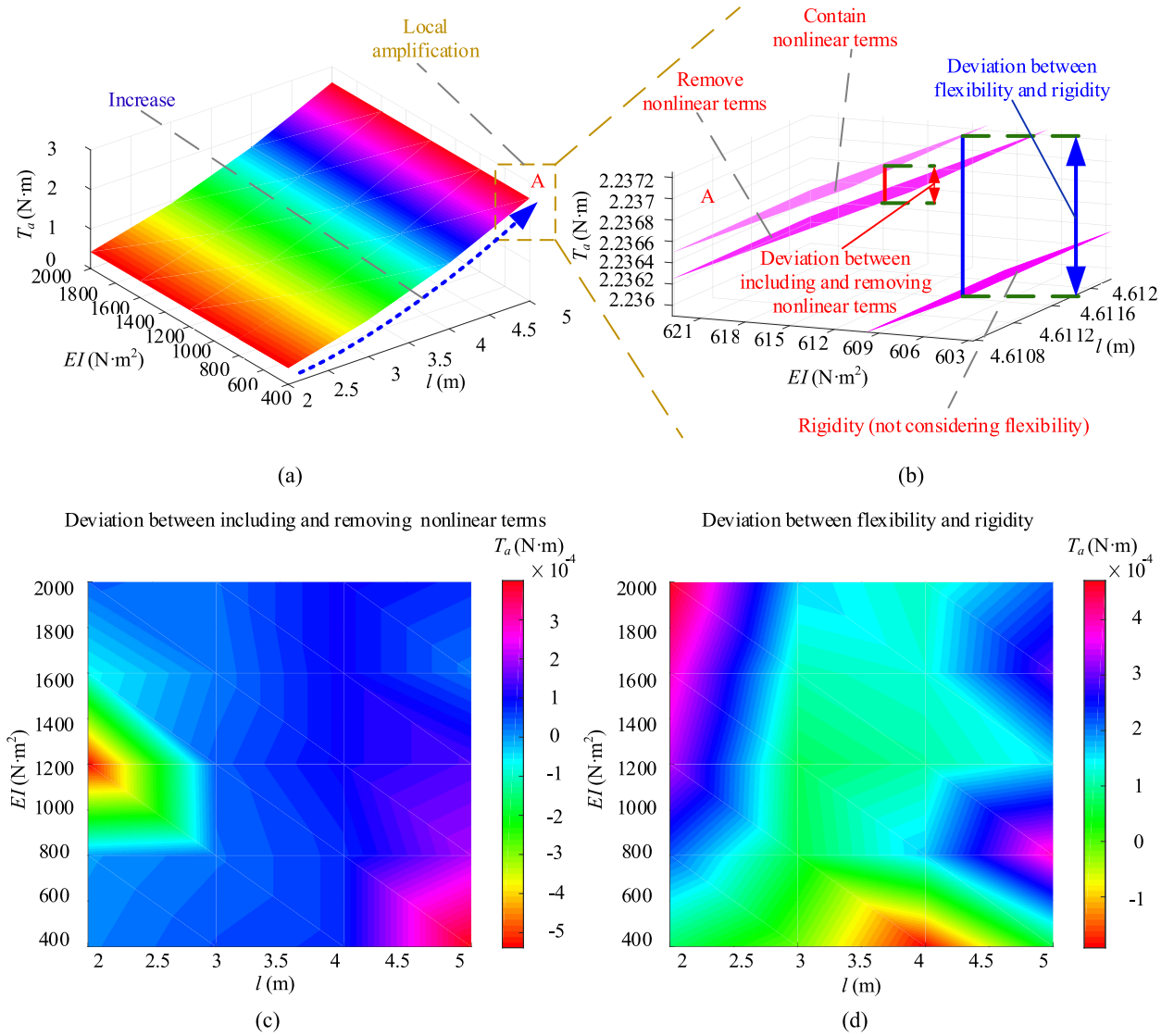

Figure 5 Input torque of flexible manipulators at low speed: (**a**) Relationship between input torque, length, and flexural rigidity, (**b**) Partial enlarged view of (**a**), (**c**) Influence of nonlinear terms on input torque, (**d**) Influence of flexibility on input torque

According to Figures 4 and 5, the following conclusions can be drawn:

1. The input torque of the flexible manipulators increases as the manipulator's length increase, but the flexural rigidity has negligible effect on the input torque.
2. Regarding low-speed movement, the input torque deviation with and without nonlinear terms is negligible. In contrast, the input torque's deviation gradually increases as the speed of the flexible manipulators increases.
3. With an increase in the manipulator's length, the input torque deviation increases gradually.

In summary, according to the above conclusions, when the manipulator is long and in a high-speed movement state, the input torque's deviation caused by nonlinear terms cannot be ignored. In this situation, the nonlinear terms should be fully considered.

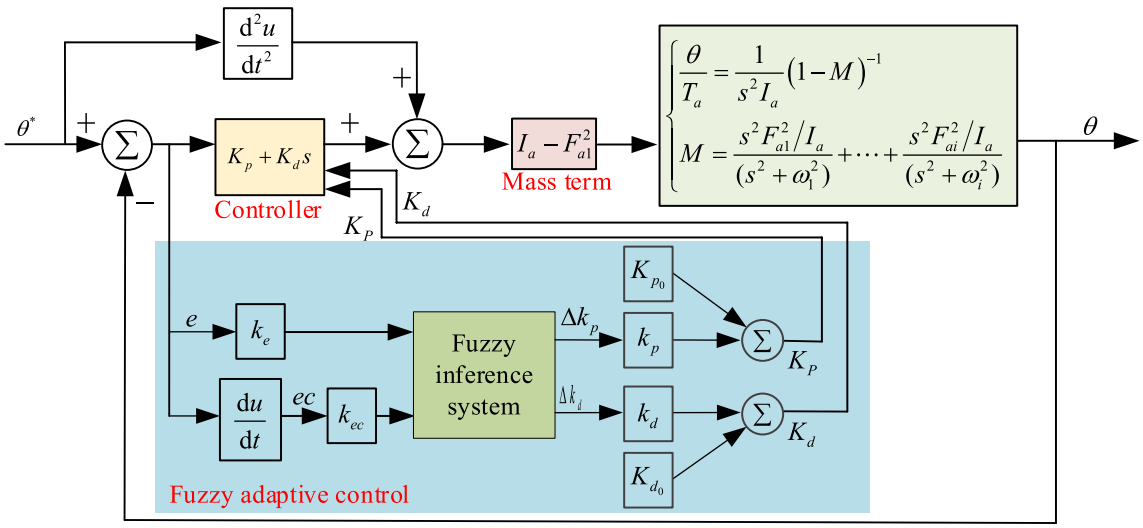

Figure 6 Control block diagram of the flexible manipulator servo system based on fuzzy adaptive adjustment

3 Combined Control Strategy Based on Fuzzy Adjustment and RBF Neural Network

3.1 Variable Range of Feedforward PD Controller Parameters

If the influence of the nonlinear terms is ignored, the transfer function of the flexible manipulator's servo system can be expressed as:

$$\begin{cases} \dfrac{\theta}{T_a} = \dfrac{1}{s^2 I_a}(1-M)^{-1}, \\ M = \dfrac{s^2 F_{a1}^2/I_a}{(s^2+\omega_1^2)} + \dfrac{s^2 F_{a2}^2/I_a}{(s^2+\omega_2^2)} + \dfrac{s^2 F_{a3}^2/I_a}{(s^2+\omega_3^2)} + \cdots + \dfrac{s^2 F_{ai}^2/I_a}{(s^2+\omega_i^2)}. \end{cases} \tag{12}$$

When only the first mode is considered, Eq. (13) can be obtained as follows:

$$\ddot{\theta} = T_a \left(\frac{1}{I_a - F_{a1}^2}\delta(t) - \frac{F_{a1}^2 \omega_1 \sin\left(\frac{\omega_1\sqrt{I_a}}{\sqrt{F_{a1}^2 - I_a}}t\right)}{\left(F_{a1}^2 - I_a\right)^{3/2}\sqrt{I_a}} i \right). \tag{13}$$

Ignoring the influence of the imaginary part and retaining the real part, Eq. (13) can be expressed as:

$$\ddot{\theta} = T_a \left(\frac{1}{I_a - F_{a1}^2} \right). \tag{14}$$

The servo control system of the flexible manipulators adopts a feedforward PD control strategy, and the PD controller parameters are adjusted using fuzzy rules. The control block diagram of the flexible manipulator servo system based on fuzzy adaptive adjustment when the nonlinear terms are ignored is illustrated in Figure 6. According to Eq. (14), the mass term in the control block diagram can be determined.

According to the control block diagram illustrated in Figure 6, the control law of the servo system can be obtained as expressed by Eq. (15).

$$\begin{cases} \tau = \left(I_a - F_{a1}^2\right)\left(\ddot{\theta}^* + K_p e + K_d \dot{e}\right), \\ e = \theta^* - \theta, \end{cases} \tag{15}$$

where θ^* and e denote the desired output and error.

Similarly, the closed-loop transfer function of the flexible manipulator servo system can be obtained according to Figure 7, as expressed in Eq. (16), where K_p and K_d are the PD control parameters.

When only the first-order model is considered, the transfer function of the flexible manipulator servo system is expressed by Eq. (17).

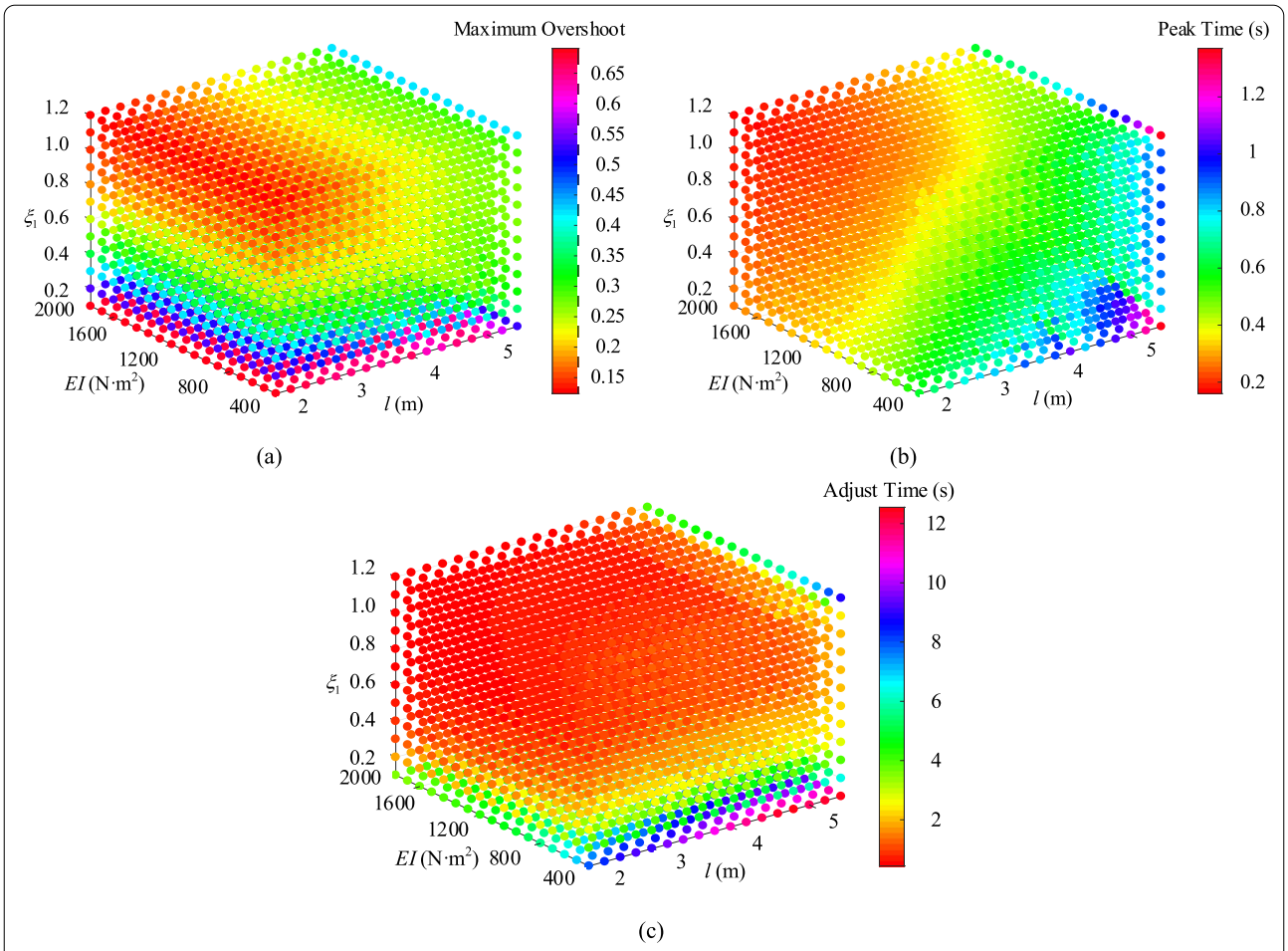

Figure 7 Distribution diagram of evaluation indexes: (**a**) Maximum overshoot, (**b**) Peak time, (**c**) Adjust time

$$G_b(s)=\frac{\left(1+\frac{s^2}{K_p+K_ds}\right)\left(K_p+K_ds\right)\left(I_a-F_{a1}^2\right)\left(\frac{1}{s^2I_a}\left(1-\sum_{i=1}^{\infty}\frac{s^2F_{ai}^2/I_a}{(s^2+\omega_i^2)}\right)^{-1}\right)}{1+\left(K_p+K_ds\right)\left(I_a-F_{a1}^2\right)\left(\frac{1}{s^2I_a}\left(1-\sum_{i=1}^{\infty}\frac{s^2F_{ai}^2/I_a}{(s^2+\omega_i^2)}\right)^{-1}\right)}, \tag{16}$$

$$\begin{aligned}G_b(s)&=\frac{\left(K_p+K_ds\right)\left(I_a-F_{a1}^2\right)\left(\frac{1}{s^2I_a}\left(1-\frac{s^2F_{ai}^2/I_a}{(s^2+\omega_i^2)}\right)^{-1}\right)+s^2\left(I_a-F_{a1}^2\right)\left(\frac{1}{s^2I_a}\left(1-\frac{s^2F_{ai}^2/I_a}{(s^2+\omega_i^2)}\right)^{-1}\right)}{1+\left(K_p+K_ds\right)\left(I_a-F_{a1}^2\right)\left(\frac{1}{s^2I_a}\left(1-\frac{s^2F_{ai}^2/I_a}{(s^2+\omega_i^2)}\right)^{-1}\right)}\\&=\frac{\left(I_a-F_{a1}^2\right)\left(s^4+K_ds^3+\left(K_p+\omega_i^2\right)s^2+K_d\omega_i^2s+K_p\omega_i^2\right)}{\omega_i^2s^2+\left(I_a-F_{a1}^2\right)\left(s^4+K_ds^3+K_ps^2+K_d\omega_i^2s+K_p\omega_i^2\right)}.\end{aligned} \tag{17}$$

According to Ref. [32], the pole placement method is employed to configure the poles of the closed-loop transfer function. The denominator polynomial in Eq. (17) can be expressed in Eq. (18).

$$\begin{cases} \omega_i^2 s^2 + \left(I_a - F_{a1}^2\right)\left(s^4 + K_d s^3 + K_p s^2 + K_d \omega_i^2 s + K_p \omega_i^2\right) = \left(I_a - F_{a1}^2\right) D, \\ D = \left(s^2 + 2\xi_{a1}\omega_{a1} s + \omega_{a1}^2\right)\left(s^2 + 2\xi_{b1}\omega_{b1} s + \omega_{b1}^2\right), \end{cases} \tag{18}$$

where ζ_{a1} and ζ_{b1} are the damping coefficients of the poles, and ω_{a1} and ω_{b1} are the natural frequency coefficients of the poles.

According to Eq. (18), Eq. (19) can be obtained:

$$\begin{cases} 2\xi_{a1}\omega_{a1} + 2\xi_{b1}\omega_{b1} = K_d, \\ \omega_{a1}^2 + \omega_{b1}^2 + 4\xi_{a1}\xi_{b1}\omega_{a1}\omega_{b1} = K_p + \dfrac{\omega_1^2}{I_a - F_{a1}^2}, \\ 2\xi_{a1}\omega_{a1}\omega_{b1}^2 + 2\xi_{b1}\omega_{b1}\omega_{a1}^2 = K_d\omega_1^2, \\ \omega_{a1}^2\omega_{b1}^2 = K_p\omega_1^2. \end{cases} \tag{19}$$

Using the pole placement method with the same damping coefficients, Eq. (20) can be obtained after sorting.

$$\begin{cases} \omega_1^2 = \omega_{a1}\omega_{b1}, \\ \left(\dfrac{\omega_{a1}^2 + \omega_{b1}^2}{\omega_{a1}\omega_{b1}}\right) + 4\xi_1^2 = 1 + \dfrac{1}{\left(I_a - F_{a1}^2\right)}. \end{cases} \tag{20}$$

According to Eq. (20), Eq. (21) can be obtained:

$$\begin{cases} \left(\dfrac{\omega_{a1}}{\omega_1} + \dfrac{\omega_1}{\omega_{a1}}\right)^2 - 2 = 1 + \dfrac{1}{\left(I_a - F_{a1}^2\right)} - 4\xi_1^2, \\ \left(\dfrac{\omega_{a1}}{\omega_1} - \dfrac{\omega_1}{\omega_{a1}}\right)^2 + 2 = 1 + \dfrac{1}{\left(I_a - F_{a1}^2\right)} - 4\xi_1^2. \end{cases} \tag{21}$$

According to Eq. (21), Eq. (22) can be obtained:

$$\begin{cases} \omega_{a1} = \dfrac{\sqrt{\frac{1}{\left(I_a - F_{a1}^2\right)} - 4\xi_1^2 + 3} + \sqrt{\frac{1}{\left(I_a - F_{a1}^2\right)} - 4\xi_1^2 - 1}}{2}\omega_1, \\ \omega_{b1} = \dfrac{\sqrt{\frac{1}{\left(I_a - F_{a1}^2\right)} - 4\xi_1^2 + 3} - \sqrt{\frac{1}{\left(I_a - F_{a1}^2\right)} - 4\xi_1^2 - 1}}{2}\omega_1. \end{cases} \tag{22}$$

According to Eq. (22), the expression for the parameters in the PD controller can be obtained as:

$$\begin{cases} K_d = 2\xi_1\omega_1\sqrt{\dfrac{1}{\left(I_a - F_{a1}^2\right)} - 4\xi_1^2 + 3}, \\ K_p = \omega_1^2. \end{cases} \tag{23}$$

Parameters such as the damping coefficient of the poles, flexible manipulator's length, and flexural rigidity affect the output of the servo system. Regarding the unit step input, this study selects the maximum overshoot, adjustment time, and peak time to evaluate the output of the servo system. The influence of the damping coefficient of the poles and manipulator parameters on the system evaluation index is obtained through a simulation, as illustrated in Figure 7.

According to Figure 7, as the damping coefficient of the poles increases, the maximum overshoot of the system gradually decreases. However, the damping coefficient of the poles has negligible effect on the peak and adjustment times. The flexural rigidity and length of the manipulators

Table 1 Fuzzy control rule table of ΔK_p

ΔK_p		*e*						
		NB	**NM**	**NS**	**ZE**	**PS**	**PM**	**PB**
ec	NB	PB	PB	PM	PM	PS	PS	ZE
	NM	PB	PM	PS	PS	NS	NS	ZE
	NS	PM	PM	PS	PS	NS	NS	ZE
	ZE	ZE	ZE	ZE	ZE	ZE	ZE	ZE
	PS	NS	NS	NS	PS	NS	NM	NB
	PM	NS	NS	NS	PS	PS	PM	PB
	PB	PS	PS	NS	PB	PM	PB	PB

Table 2 Fuzzy control rule table of ΔK_d

ΔK_d		*e*						
		NB	**NM**	**NS**	**ZE**	**PS**	**PM**	**PB**
ec	NB	PS	PS	ZE	ZE	ZE	PB	PB
	NM	NS	NS	NS	ZE	PS	PM	PM
	NS	PS	PS	PS	ZE	PS	PS	PS
	ZE	PS	PS	PS	ZE	PS	PS	PS
	PS	PS	PS	PS	ZE	PS	PS	PS
	PM	PM	PM	PS	ZE	PS	PM	PM
	PB	PB	PM	PS	ZE	PS	PM	PB

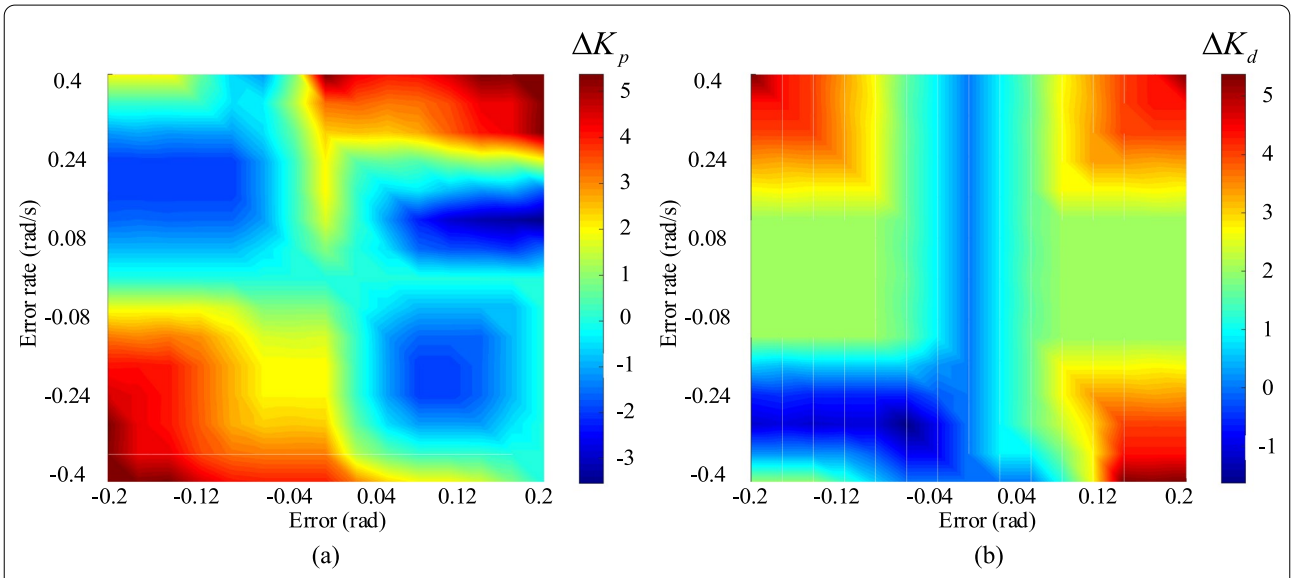

Figure 8 Distribution diagram of fuzzy inference relationship: (**a**) Distribution of Δk_p, (**b**) Distribution of Δk_d

mainly affect the peak and adjustment times. The flexural rigidity is negligible, manipulator length is increased, and manipulators have strong flexibility. When the flexibility of the manipulators increases, peak and adjustment times increase. This indicates that the system takes a long time to obtain a stable output response when the manipulators are more flexible. According to Figure 7, the damping coefficient of the poles can be appropriately selected to meet the requirement that flexible manipulators can obtain a stable output under different parameters. The damping coefficient of the poles provides a theoretical basis for determining the variation range of controller parameters.

3.2 Controller Parameter Adjustment Method Based on Fuzzy Adaptation Rules

During the movement of telescopic flexible manipulators, the parameters of the manipulators alter as their length changes. According to Eq. (23), the controller parameters at the initial and termination movements of the flexible manipulators are determined by selecting an appropriate damping coefficient for the poses. Thus, the variation range of the controller parameters is defined, and is ready for the fuzzy adaptive control strategy in the movement process. The fuzzy adaptive PD controller adopts the error and error change rate as the input, and controller parameters as the output. The fuzzy adaptive

control strategy employs fuzzy rules to adjust the controller parameters in real-time to reduce errors. According to Ref. [24], the fuzzy domain of the output variables is [−6, 6]. The domain of the actual input error is set to [−0.1, 0.1], and the domain of the actual input error rate of change is [−0.2, 0.2]. Based on this, the error, error rate of change, and quantization factor of the controller parameters is obtained. The fuzzy sets of the input and output of the fuzzy controller are set to six as follows:

$$e, ec, \Delta k_p, \Delta k_d = \{\text{ NB NM NS ZE PS PM PB }\}, \tag{24}$$

where N = positive, and P = negative; B = large; M = moderate; S = small, and ZE= zero.

The triangle function is selected as the membership function of the input and output variables of the fuzzy controller in this study. According to Ref. [24], the fuzzy rule table of the PD control parameters can be determined, as shown in Tables 1 and 2. Thus, a fuzzy inference relationship is obtained, as shown in Figure 8.

According to the fuzzy inference relationship, the parameters of the PD control can be determined by Eq. (25).

$$\begin{cases} K_d = K_{d_0} + k_d \Delta k_d, \\ K_P = K_{P_0} + k_p \Delta k_p, \\ K_{d0} = 2\xi_{10}\omega_{10}\sqrt{\dfrac{1}{(I_{a0} - F_{a10}^2)} - 4\xi_{10}^2 + 3}, \\ K_{p0} = \omega_{10}^2, \\ K_{dn} = 2\xi_{1n}\omega_{1n}\sqrt{\dfrac{1}{(I_{an} - F_{a1n}^2)} - 4\xi_{1n}^2 + 3}, \\ K_{pn} = \omega_{1n}^2, \\ k_d = \dfrac{K_{dn} - K_{d0}}{6}, \\ k_p = \dfrac{K_{pn} - K_{p0}}{6}, \end{cases} \tag{25}$$

where ω_{10} and ω_{1n} represent the modal frequencies of flexible manipulators at the initial and termination movements; I_{a0} and I_{an} represent the inertia of flexible manipulators at the initial and termination movements; F_{a10} and F_{a1n} represent the modal coupling coefficients of flexible manipulators at the initial and termination movements; K_{d0}, K_{dn} , K_{p0} and K_{pn} represent the controller parameters at the initial and termination movements; ΔK_d and ΔK_p represent the fuzzy rule output.

3.3 Identification of Uncertain Part of Flexible Manipulator Based on RBF Neural Network

Telescopic flexible manipulators cannot ignore the influence of nonlinear terms when the manipulator's length is long and rotation speed is high. In addition, the dynamic parameters of telescopic flexible manipulators are time-varying in the processes of movement. Therefore, the uncertain part of the servo system for telescopic flexible manipulators comprises nonlinear terms and time-varying characteristics of the parameters. In this study, the RBF neural network is utilized to identify the uncertain parts of telescopic flexible manipulators. In addition, the uncertain part after identification is compensated for by the control law, thereby improving the movement accuracy of telescopic flexible manipulators.

According to Eqs. (9) and (14), the dynamic equation of telescopic flexible manipulators is expressed the form indicated in Eq. (26).

$$\begin{cases} \ddot{\theta}\left(I_a - F_{a1}^2\right) = T_a + d, \\ d = -\ddot{\theta}\sum_{i=1}^{\infty}\delta_i(t)^2 - 2\dot{\theta}\sum_{i=1}^{\infty}\delta_i(t)\dot{\delta}_i(t). \end{cases} \tag{26}$$

Owing to the time-varying characteristics of the parameters of telescopic flexible manipulators in the movement processes, accurate system parameters cannot be obtained. Therefore, only nominal models can be established. The control law for the nominal model is expressed by Eq. (27).

$$\tau = \left(\hat{I}_a - \hat{F}_{a1}^2\right)\left(\ddot{\theta}^* + K_d\dot{e} + K_p e\right), \tag{27}$$

where $\hat{I}_a$ and $\hat{F}_{a1}$ represent the nominal inertia and nominal first-order modal coupling coefficient, respectively.

By substituting the control law of the nominal model into Eq. (26), Eq. (28) can be obtained.

$$\left(\hat{I}_a - \hat{F}_{a1}^2\right)\left(\ddot{\theta}^* + K_d\dot{e} + K_p e\right) = \ddot{\theta}\left(I_a - F_{a1}^2\right) - d. \tag{28}$$

After simplifying Eq. (28), Eq. (29) can be obtained.

$$\begin{aligned} &\left(\hat{I}_a - \hat{F}_{a1}^2\right)\left[\left(\ddot{\theta}^* - \ddot{\theta}\right) + K_d\dot{e} + K_p e\right] = \\ &\ddot{\theta}\left[\left(I_a - F_{a1}^2\right) - \left(\hat{I}_a - \hat{F}_{a1}^2\right)\right] - d \quad . \end{aligned} \tag{29}$$

According to Eq. (29), the error state equation of the system can be obtained as

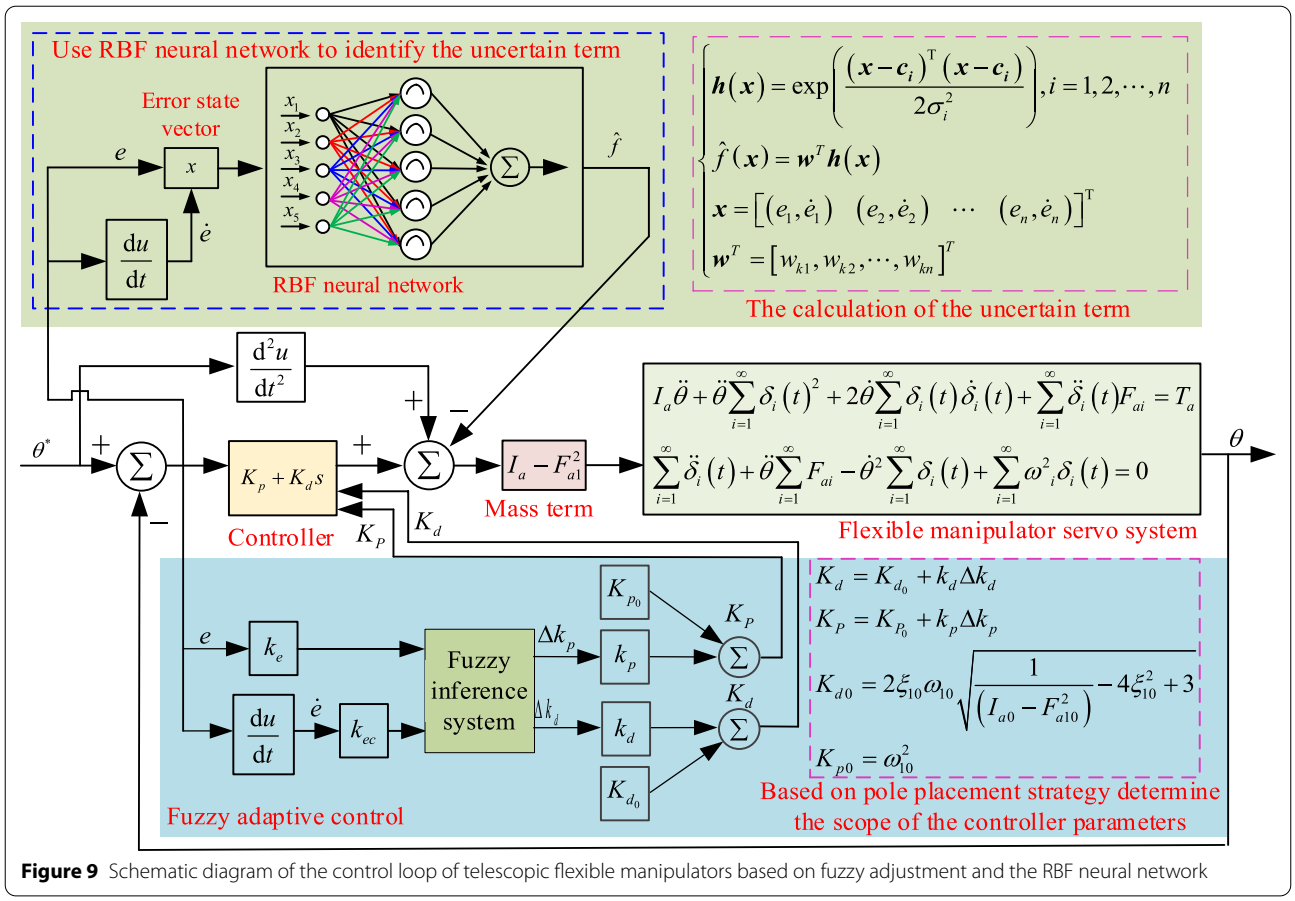

Figure 9 Schematic diagram of the control loop of telescopic flexible manipulators based on fuzzy adjustment and the RBF neural network

$$\begin{cases} \ddot{e} + K_d\dot{e} + K_p e = \left(\hat{I}_a - \hat{F}_{a1}^2\right)^{-1}\left(\ddot{\theta}\Delta\left(I_a - F_{a1}^2\right) - d\right) \\ \Delta\left(I_a - F_{a1}^2\right) = \left(I_a - F_{a1}^2\right) - \left(\hat{I}_a - \hat{F}_{a1}^2\right) \end{cases} \tag{30}$$

According to Eq. (30), the uncertain part due to the time-varying characteristics of the model parameters and nonlinear terms can be obtained, and the expression is as follows:

$$f = \left(\hat{I}_a - \hat{F}_{a1}^2\right)^{-1}\left(\ddot{\theta}\Delta\left(I_a - F_{a1}^2\right) - d\right) \tag{31}$$

According to Eq. (31), the error state equation of the system can be expressed as:

$$\ddot{\theta}^* + K_d\dot{e} + K_p e - f = \ddot{\theta} \tag{32}$$

Assuming that the uncertain part is known, the control law of the servo system can be obtained as

$$\tau = \left(\hat{I}_a - \hat{F}_{a1}^2\right)\left(\ddot{\theta}^* + K_d\dot{e} + K_p e - f\right) \tag{33}$$

Because the parameters of flexible manipulators have time-varying characteristics, the uncertainty part cannot be obtained. Therefore, it is necessary to identify the uncertain part. In this study, an RBF neural network is utilized to identify the uncertain part. The error and error change rate are taken as the inputs of the neural network, and the uncertain part after identification is taken as the output. According to Ref. [28], the algorithm of the RBF neural network is as follows:

$$\begin{cases} \boldsymbol{h}(\boldsymbol{x}) = \exp\left(\dfrac{(x - c_i)^{\mathrm{T}}(\boldsymbol{x} - c_i)}{2\sigma_i^2}\right), i = 1, 2, \cdots, n, \\ \hat{f}(\boldsymbol{x}) = \boldsymbol{w}^{\mathrm{T}}\boldsymbol{h}(\boldsymbol{x}), \\ f = \hat{f}(\boldsymbol{x}) + \varepsilon, \\ \boldsymbol{x} = \left[\ (e_1, \dot{e}_1)\ \ (e_2, \dot{e}_2)\ \ \cdots\ \ (e_n, \dot{e}_n)\ \right]^{\mathrm{T}}, \\ \boldsymbol{w}^{\mathrm{T}} = [w_{k1}, w_{k2}, \cdots, w_{kn}]^{\mathrm{T}}, \end{cases} \tag{34}$$

where $\boldsymbol{x}$ represents the input of the RBF neural network, which comprises the error and error change rate, $\boldsymbol{h}(\boldsymbol{x})$ represents the output of the hidden nodes of the neural network, $\boldsymbol{w}$ represents the vector of the neural network weight coefficients, $\hat{f}(\boldsymbol{x})$ represents the output value of

the neural network after identification, and ε represents the error between the uncertainty part identified by the neural network and actual uncertainty part.

After using the RBF neural network to identify the uncertain part, the new control law is expressed as:

$$\tau = \left(\hat{I}_a - \hat{F}_{a1}^2\right)\left(\ddot{\theta}^* + K_d\dot{e} + K_p e - \hat{f}(\boldsymbol{x})\right). \tag{35}$$

The parameters of the controller are adjusted in real time according to the fuzzy rules. Based on the use of fuzzy rules to adjust the controller parameters, the RBF neural network is utilized to identify the uncertain part of the telescopic flexible manipulators. The control loop diagram of the telescopic flexible manipulator's servo system based on fuzzy adjustment and RBF neural network is illustrated in Figure 9.

3.4 Stability Proof

After utilizing the RBF neural network to identify the uncertain part of the telescopic flexible manipulators, the control law is obtained, as expressed in Eq. (35). According to Eq. (35), the error state equation of the system can be obtained as:

$$\ddot{e} + K_d\dot{e} + K_p e = \hat{f}(\boldsymbol{x}) - f. \tag{36}$$

According to Eq. (36), Eq. (37) can be obtained as:

$$\begin{cases} \dot{\boldsymbol{E}} = \boldsymbol{\Lambda E} + \boldsymbol{b}\left(\hat{f}(\boldsymbol{x}) - f\right), \\ \boldsymbol{E} = \begin{bmatrix} e & \dot{e} \end{bmatrix}^{\mathrm{T}}, \\ \boldsymbol{\Lambda} = \begin{bmatrix} 0 & 1 \\ -K_p & -K_d \end{bmatrix}, \\ \boldsymbol{b} = \begin{bmatrix} 0 & 1 \end{bmatrix}^{\mathrm{T}}. \end{cases} \tag{37}$$

Assume that the optimal neural network weight coefficient vector satisfies:

$$\boldsymbol{w}^* = \arg\min_{\boldsymbol{w}\in\Omega}\left[\sup\left|\hat{f}(\boldsymbol{x}) - f\right|\right], \tag{38}$$

where Ω is the set of $\boldsymbol{w}$ and $\boldsymbol{w}^*$ represents the optimal neural network weight coefficient.

It is assumed that the minimum error between the real and identified uncertain parts of the RBF neural network satisfies the following:

$$\varepsilon^* = \hat{f}\left(\boldsymbol{x}\middle|\boldsymbol{w}^*\right) - f. \tag{39}$$

By substituting Eq. (39) into Eq. (37), the error state equation of the system can be obtained as:

$$\begin{cases} \dot{E} = \boldsymbol{\Lambda} E + b\left(\hat{f}(x) - \hat{f}\left(x\middle|w^*\right) + \varepsilon^*\right) \\ \quad = \boldsymbol{\Lambda} E + b\left(\left(w - w^*\right)^{\mathrm{T}} h(x) + \varepsilon^*\right) \\ \quad = \Lambda E + M, \\ M = b\left(\left(w - w^*\right)^{\mathrm{T}} h(x) + \varepsilon^*\right). \end{cases} \tag{40}$$

According to Eq. (40), the relation between the error and weight coefficient of the neural network can be obtained. The error can be minimized by designing an adaptive law for the weight coefficient of the neural network.

Define the Lyapunov function as:

$$\begin{cases} V = V_1 + V_2, \\ V_1 = \dfrac{1}{2}\boldsymbol{E}^{\mathrm{T}}\boldsymbol{P}\boldsymbol{E}, \\ V_2 = \dfrac{1}{2\gamma}\left[\left(\boldsymbol{w} - \boldsymbol{w}^*\right)^{\mathrm{T}}\left(\boldsymbol{w} - \boldsymbol{w}^*\right)\right], \end{cases} \tag{41}$$

where γ is a positive number, and $\boldsymbol{P}$ is a tuning matrix that satisfies the Lyapunov equation expressed as:

$$\boldsymbol{\Lambda}^{\mathrm{T}}\boldsymbol{P} + \boldsymbol{P}\boldsymbol{\Lambda} = -\boldsymbol{Q}. \tag{42}$$

Deriving the Lyapunov function, Eq. (43) holds.

$$\begin{cases} \dot{V}_1 = \dfrac{1}{2}\dot{E}^{\mathrm{T}}PE + \dfrac{1}{2}E^{\mathrm{T}}P\dot{E} = \dfrac{1}{2}\left(E^{\mathrm{T}}\boldsymbol{\Lambda}^{\mathrm{T}} + M^{\mathrm{T}}\right)PE \\ \qquad + \dfrac{1}{2}E^{\mathrm{T}}P(\boldsymbol{\Lambda}E + M) \\ = \dfrac{1}{2}E^{\mathrm{T}}\left(\boldsymbol{\Lambda}^{\mathrm{T}}P + P\boldsymbol{\Lambda}\right)E + \dfrac{1}{2}M^{\mathrm{T}}PE + \dfrac{1}{2}E^{\mathrm{T}}PM \\ = -\dfrac{1}{2}E^{\mathrm{T}}QE + E^{\mathrm{T}}Pb\left(w - w^*\right)^{\mathrm{T}}h(x) + E^{\mathrm{T}}Pb\varepsilon^*, \\ \dot{V}_2 = \dfrac{1}{\gamma}\left(w - w^*\right)^{\mathrm{T}}\dot{w}, \\ \dot{V} = \dot{V}_1 + \dot{V}_2 \\ = -\dfrac{1}{2}E^{\mathrm{T}}QE + E^{\mathrm{T}}Pb\left(w - w^*\right)^{\mathrm{T}}h(x) \\ \qquad + E^{\mathrm{T}}Pb\varepsilon^* + \dfrac{1}{\gamma}\left(w - w^*\right)^{\mathrm{T}}\dot{w} \\ = -\dfrac{1}{2}E^{\mathrm{T}}QE + E^{\mathrm{T}}Pb\varepsilon^* \\ \qquad + \dfrac{1}{\gamma}\left(w - w^*\right)^{\mathrm{T}}\left[\dot{w} + \gamma E^{\mathrm{T}}Pbh(x)\right]. \end{cases} \tag{43}$$

We assume that the adaptive law of the weight coefficients of the neural network is expressed as:

$$\dot{\boldsymbol{w}} = -\gamma\boldsymbol{E}^{\mathrm{T}}\boldsymbol{P}\boldsymbol{b}\boldsymbol{h}(\boldsymbol{x}). \tag{44}$$

Substitute Eq. (44) into Eq. (43) to obtain:

$$\dot{V} = -\frac{1}{2}\boldsymbol{E}^{\mathrm{T}}\boldsymbol{Q}\boldsymbol{E} + \boldsymbol{E}^{\mathrm{T}}\boldsymbol{P}\boldsymbol{b}\varepsilon^{*}. \tag{45}$$

According to the properties of the matrix, Eq. (46) holds.

$$2\boldsymbol{E}^{\mathrm{T}}\boldsymbol{P}\boldsymbol{b}\varepsilon^{*} \le \psi\left(\boldsymbol{E}^{\mathrm{T}}\boldsymbol{P}\boldsymbol{b}\right)\left(\boldsymbol{E}^{\mathrm{T}}\boldsymbol{P}\boldsymbol{b}\right)^{\mathrm{T}} + \frac{1}{\psi}\varepsilon^{*2}, \tag{46}$$

where ψ is a positive number.

According to Eq. (46), Eq. (47) can be obtained:

$$\boldsymbol{E}^{\mathrm{T}}\boldsymbol{P}\boldsymbol{b}\varepsilon^{*} \le \frac{\psi}{2}\boldsymbol{E}^{\mathrm{T}}\left(\boldsymbol{P}\boldsymbol{b}\boldsymbol{b}^{\mathrm{T}}\boldsymbol{P}^{\mathrm{T}}\right)\boldsymbol{E} + \frac{1}{2\psi}\varepsilon^{*2}. \tag{47}$$

Therefore, the derivative of the Lyapunov function is expressed as:

$$\begin{aligned}\dot{V} &\le -\frac{1}{2}\boldsymbol{E}^{\mathrm{T}}\boldsymbol{Q}\boldsymbol{E} + \frac{\psi}{2}\boldsymbol{E}^{\mathrm{T}}\left(\boldsymbol{P}\boldsymbol{b}\boldsymbol{b}^{\mathrm{T}}\boldsymbol{P}^{\mathrm{T}}\right)\boldsymbol{E} + \frac{1}{2\psi}\varepsilon^{*2} \\ &= -\frac{1}{2}\boldsymbol{E}^{\mathrm{T}}\left(\boldsymbol{Q} - \psi\boldsymbol{P}\boldsymbol{b}\boldsymbol{b}^{\mathrm{T}}\boldsymbol{P}^{\mathrm{T}}\right)\boldsymbol{E} + \frac{1}{2\psi}\varepsilon^{*2} \\ &\le -\frac{1}{2}l_{\min}\left(\boldsymbol{Q} - \psi\boldsymbol{P}\boldsymbol{b}\boldsymbol{b}^{\mathrm{T}}\boldsymbol{P}^{\mathrm{T}}\right)\|\boldsymbol{E}\|^{2} + \frac{1}{2\psi}\varepsilon^{*2}.\end{aligned} \tag{48}$$

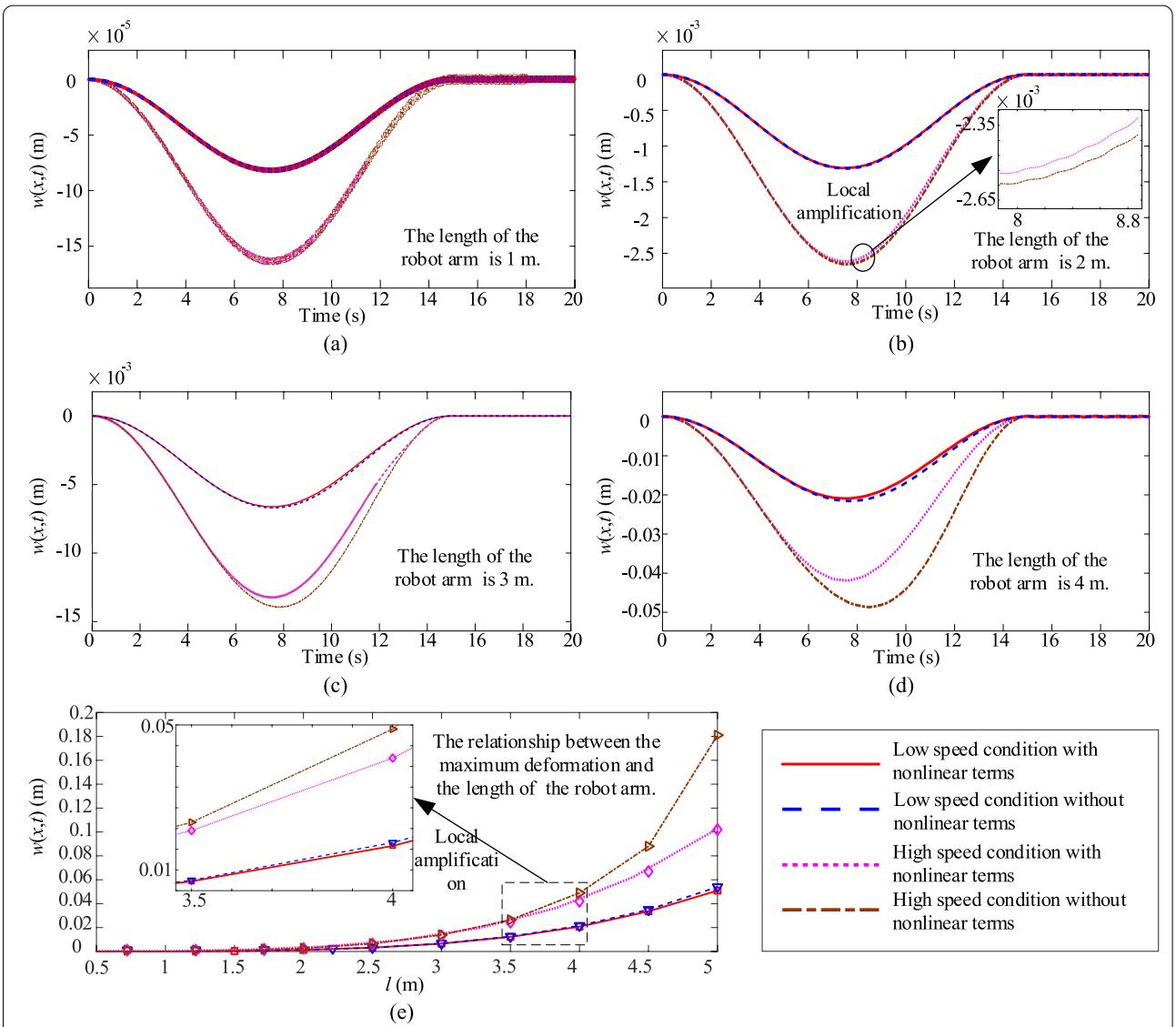

Figure 10 Influence of the manipulator's length on maximum deformation: (**a**) Simulation results when the length is 1 m, (b) Simulation results when the length is 2 m, (**c**) Simulation results when the length is 3 m, (**d**) Simulation results when the length is 4 m, (**e**) Relationship between maximum deformation and length

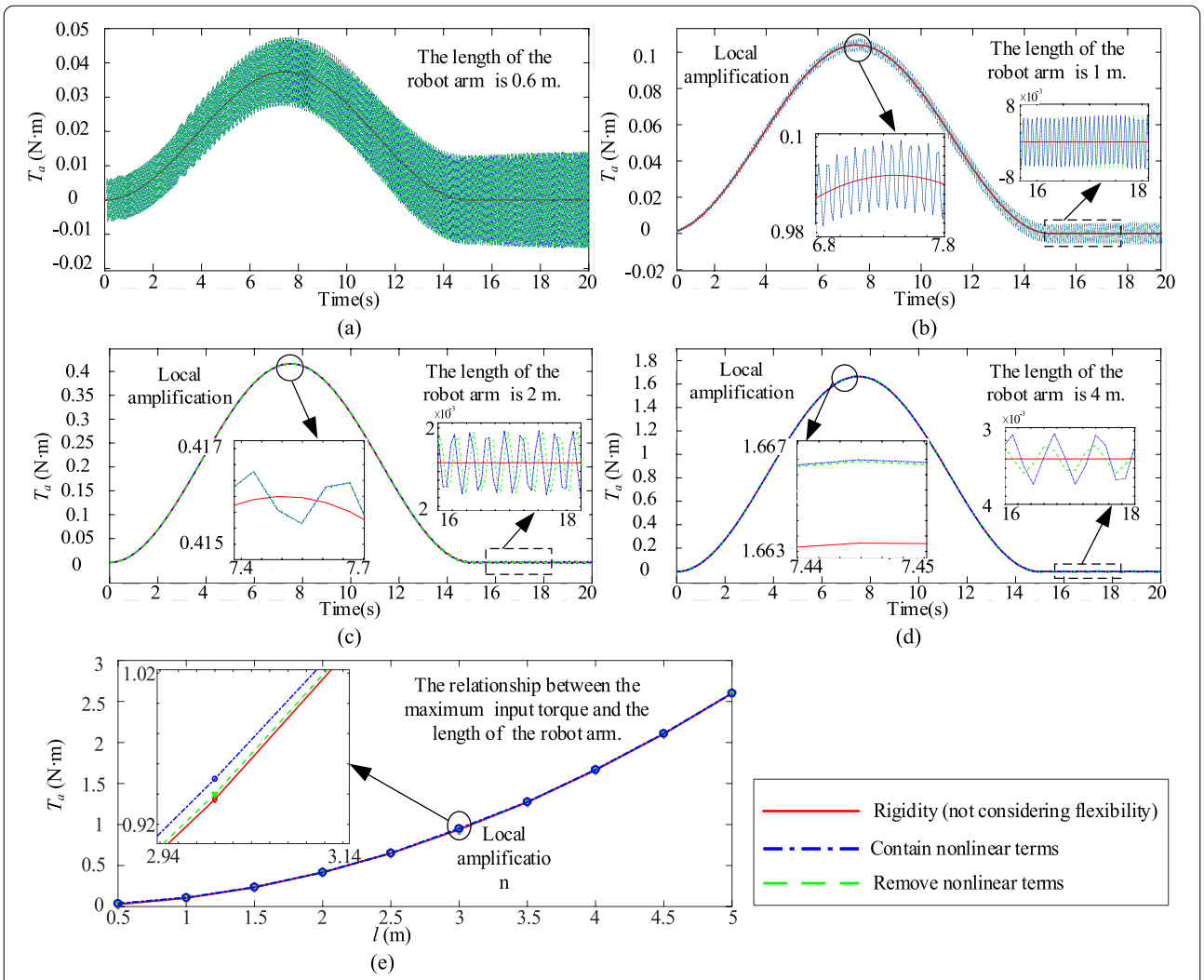

Figure 11 Influence of the manipulator's length on input torque: (**a**) Simulation results when the length is 1 m, (**b**) Simulation results when the length is 2 m, (**c**) Simulation results when the length is 3 m, (**d**) Simulation results when the length is 4 m, (**e**) Relationship between maximum input torque and length

where $l_{\min}(\cdot)$ represents the eigenvalue of the matrix.

If the derivative of the Lyapunov function is less than zero, then Eq. (49) must be satisfied.

$$\|\boldsymbol{E}\|^2 \leq \frac{|\varepsilon^*|}{\sqrt{\psi l_{\min}\left(\boldsymbol{Q} - \psi \boldsymbol{P}\boldsymbol{b}\boldsymbol{b}^{\mathrm{T}}\boldsymbol{P}^{\mathrm{T}}\right)}}. \tag{49}$$

Therefore, the eigenvalues of $\|\boldsymbol{E}\|^2$, $\boldsymbol{Q}$, and P can be appropriately selected to ensure $\dot{V} \leq 0$. In turn, the stability of the telescopic flexible manipulators is ensured.

4 Numerical Simulation and Experiment

To study the effectiveness of the control strategy based on the combination of fuzzy adjustment and RBF neural network, a numerical simulation analysis and physical prototype experiment of flexible manipulators are conducted. Because of the variable length of telescopic flexible manipulators, this study focuses on the analysis of the influence of manipulator's length on the dynamic and control performance. In this study, fuzzy adjustment and RBF neural network are employed to improve the control accuracy of flexible manipulator's rotation angles. The parameters of the feedforward PD controller are adjusted

Table 3 Parameter of flexible manipulator

Parameters	Condition 1	Condition 2	Condition 3
Length of the fixed flexible manipulator l_1(m)	2	2	2
Length of the axially translating arm l_2(m)	0.5	1	2
Flexible manipulator's length l(m)	2.5	3	4
Flexible manipulator mass m(kg)	1	1	1
Linear density of flexible manipulator ρA(kg/m^2)	0.4	0.3333	0.25
Flexural rigidity of flexible manipulator EI(N·m^2)	500	500	500
Flexible manipulator inertia J_m(kg·m^2)	2.083	3	5.33
Modal coupling coefficient F_{a1}(kg$^{1/2}$·m)	1.42	1.7064	2.2752
Characteristic root of modal function β_1	0.35	0.2916	0.46875
Damping coefficient of the poses	0.5	0.5	0.7
Controller parameters K_p	395	228	203
Controller parameters K_d	85	55	35

in real time according to fuzzy rules. The variation range of the controller parameters is determined by the manipulator's length and damping coefficient of the poles. Fuzzy rules are employed to adjust the parameters of the controller in real time. In addition, an RBF neural network is utilized to identify the uncertain part in the dynamic model of flexible manipulators. The identified uncertain part is compensated by the control law in the form of an internal control loop. The uncertain part of the flexible manipulator's model includes both flexible nonlinear terms and time-varying characteristics of the dynamic parameters. First, the influence of the manipulator's length on the dynamic characteristics is analyzed by numerical simulation. Then, simulation experiments on telescopic flexible manipulators with different lengths are conducted. Finally, control experiments on the physical prototype of the flexible manipulators are conducted. Through numerical simulations and prototype experiments, the combined control of fuzzy adjustment and the RBF neural network can be proved effectively.

4.1 Influence of Manipulators' Length on Dynamic Performance

A telescopic flexible manipulator comprises a fixed manipulator and telescopic arm. The overall length of the flexible manipulator alters during the movement of the telescopic arm. The change in the manipulator's length will not only cause a change in the dynamic parameters, but also lead to the deformation of the flexible manipulators and input torque. According to Eq. (9), the deformation of flexible manipulators considering nonlinear terms can be obtained. Similarly, according to Eq. (10), the deformation of the flexible manipulators can be obtained when the nonlinear terms are ignored. In this study, the influence of the manipulator's length on the maximum deformation is obtained through numerical simulation, as illustrated in Figure 10. The rotation angle equation expressed in Eq. (11) is indicated as the input signal. Similarly, the input torque of the flexible manipulator can be obtained using Eqs. (9) and (10). In the case of low speed, the influence of the manipulator's length on the input torque is illustrated in Figure 11.

According to Figure 10, as the length of the manipulators increase, the maximum deformation of the flexible manipulators gradually increases. When the length of the manipulators is negligible, the nonlinear terms in the dynamic equation have less influence on the maximum deformation. However, with an increase in the length of the manipulators, the influence of the nonlinear terms on the maximum deformation gradually increases, and this is especially obvious when the flexible manipulator rotates at high speed. Therefore, the influence of the nonlinear terms should be considered for flexible manipulators with high speeds and long lengths. Similarly, according to Figure 11, as the length of the manipulators increases, the input torque of the flexible manipulators must be larger. When considering the nonlinear terms, the fluctuation in the input torque of the flexible manipulators increases slightly. Flexible manipulators depend on the fluctuation of the input torque to suppress the fluctuation of the rotation angle caused by flexibility.

4.2 Combined Control Strategy Simulation

The length of the telescopic flexible manipulator alters during movement. The dynamic parameters of the telescopic flexible manipulator at three different lengths are selected as the simulation model parameters under

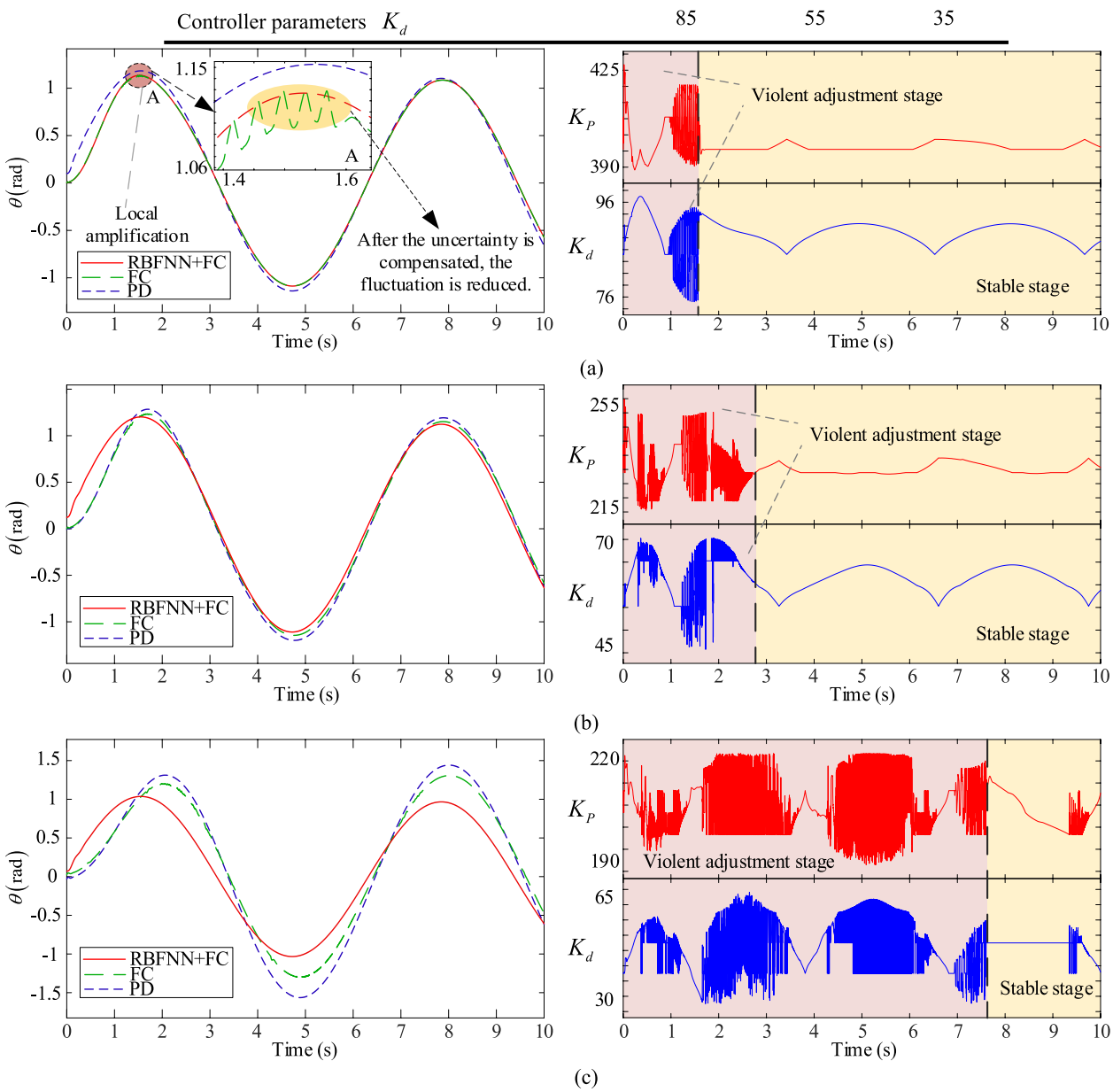

Figure 12 Output results of rotation angle of the flexible manipulator: (**a**) Output results of Condition 1, (**b**) Output results of Condition 2, (**c**) Output results of Condition 3

different working conditions, as presented in Table 3. The damping coefficients of the poles can be appropriately selected, as illustrated in Figure 7 to determine the range of controller parameter variations.

The feedforward PD control, fuzzy control, and combined control strategies are employed to control the flexible manipulator under three different working conditions. The sine signal is taken as the input signal to obtain the output result of the rotation angle of the flexible manipulator, as illustrated in Figure 12.

According to Figure 12, the control strategy based on the combination of fuzzy adjustment and the RBF neural network can realize the stable tracking of flexible manipulators. When the length of the flexible manipulators is short, the tracking effects of the three control strategies are not significantly different. However, as the length of the manipulators increases, the flexibility gradually increases, and the feedforward PD and fuzzy control strategies cannot guarantee a good tracking effect.

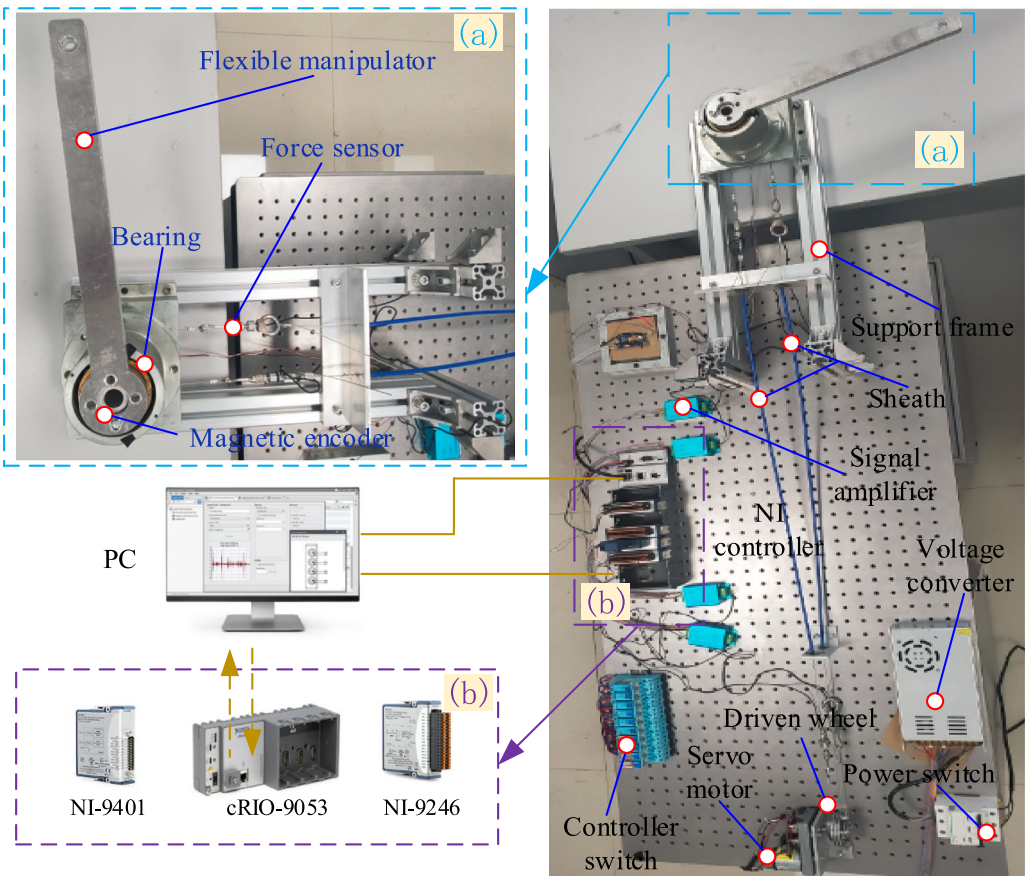

Figure 13 Experimental control platform of the flexible manipulator

From the adjustment time of the controller parameters, it can be observed that as the length of the manipulators increases, the control of the flexible manipulator gradually becomes difficult. The combined control strategy can effectively reduce the rotation angle fluctuation of flexible manipulators and improve control accuracy.

4.3 Control Experiment of Flexible Manipulator

To verify the effectiveness of the proposed control strategy, an experimental platform for a flexible manipulator is built, as illustrated in Figure 13. The flexible manipulator experimental platform comprises a flexible manipulator, NI controller, servo motor, and transmission device. The rotation angle of the flexible manipulator is measured by the encoder and collected by the NI9401 module to enter the control system in real time. The control system transmits voltage signals to the servo motor in real time through the NI9246 module, and the servo motor is controlled by the voltage. The control program is written using LabVIEW software and compiled using the Can interface of cRIO-9503 to control the rotation of the flexible manipulator.

The experimental platform simulates telescopic flexible manipulators under different conditions by altering flexible loads of different lengths. Taking a flexible load with a length of 1 m as an example, different control strategies are employed to control the rotation angle of the flexible manipulator. Using a sinusoidal function as the input signal, the output rotation angle of the flexible load under different control strategies is illustrated in Figure 14.

As illustrated in Figure 14, when the length of the flexible manipulator is 1 m, the three control strategies can achieve good tracking. However, the control strategy based on the combination of fuzzy adjustment and the RBF neural network has more negligible errors. Therefore, this control strategy can effectively improve the control accuracy of the flexible manipulators.

The length of the telescopic flexible manipulator alters during movement. To simulate the control effect of a flexible manipulator with different lengths, this study adopts flexible loads with lengths of 0.5, 1, 1.5 and 2 m to conduct the control experiment. The distribution of the rotation angle error data for flexible loads with

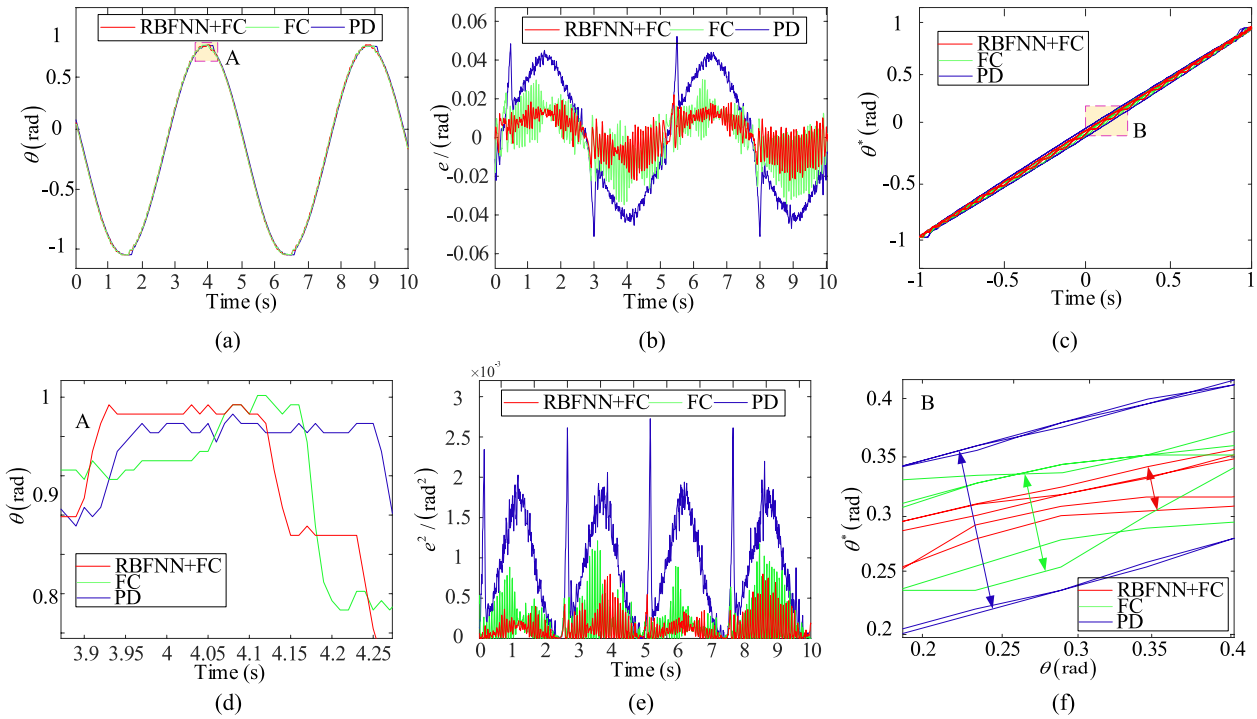

Figure 14 Output results under different control strategies when the length of the flexible manipulator is 1 m: (**a**) Rotation angle curve, (**b**) Error curve, (**c**) Relationship between input and output, (**d**) Partial enlarged view of (**a**), (**e**) Error quadratic curve, (**f**) Partial enlarged view of (**c**)

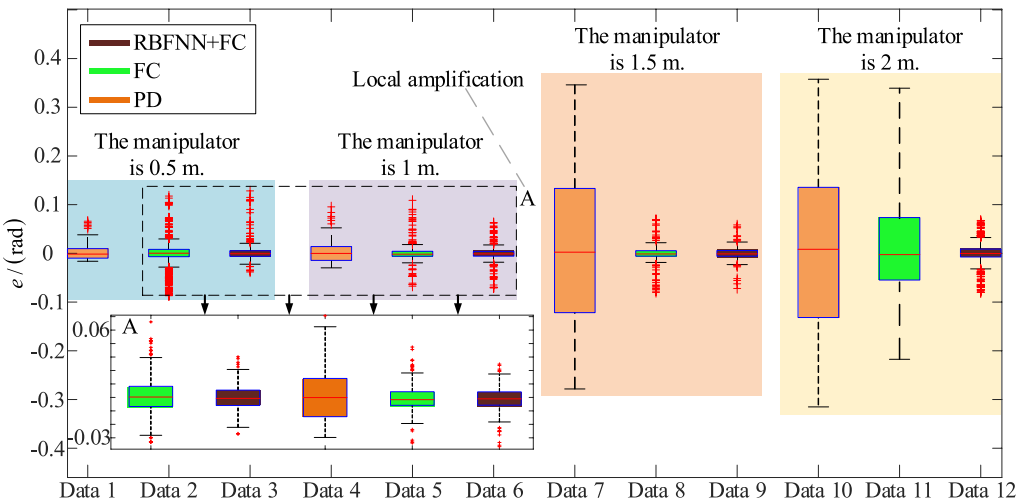

Figure 15 Rotation angle error distribution diagram of flexible manipulators

different lengths is obtained, as illustrated in Figure 15. The data of the errors are analyzed, and the results are presented in Table 4. In Table 4, four indices of means, variances, standard deviations of errors, and means of absolute errors are adopted for statistical analysis of the error data. The error evaluation indices in Table 4 are presented graphically, as illustrated in Figure 16.

According to Figure 15, as the flexible manipulator's length increases, the errors of the feedforward PD and

Table 4 Evaluation index of experimental error

Flexible manipulator's length (m)	Control strategy	Means of errors	Means of absolute errors	Variance of errors	Standard deviation of errors
0.5	PD	0.0016	0.0355	0.0054	0.0734
	FC	0.0038	0.0226	0.0025	0.0501
	RNFNN+FC	0.0023	0.0151	0.0011	0.0377
1	PD	0.0024	0.0235	0.0091	0.0956
	FC	0.0053	0.0322	0.0040	0.0634
	RNFNN+FC	0.0018	0.0159	0.0017	0.0407
1.5	PD	0.0033	0.2359	0.0695	0.2636
	FC	0.0033	0.0173	0.0027	0.0516
	RNFNN+FC	0.0021	0.0157	0.0017	0.0415
2	PD	0.0013	0.2634	0.1044	0.3230
	FC	0.0034	0.2420	0.0773	0.2781
	RNFNN+FC	0.0029	0.0602	0.0324	0.1800

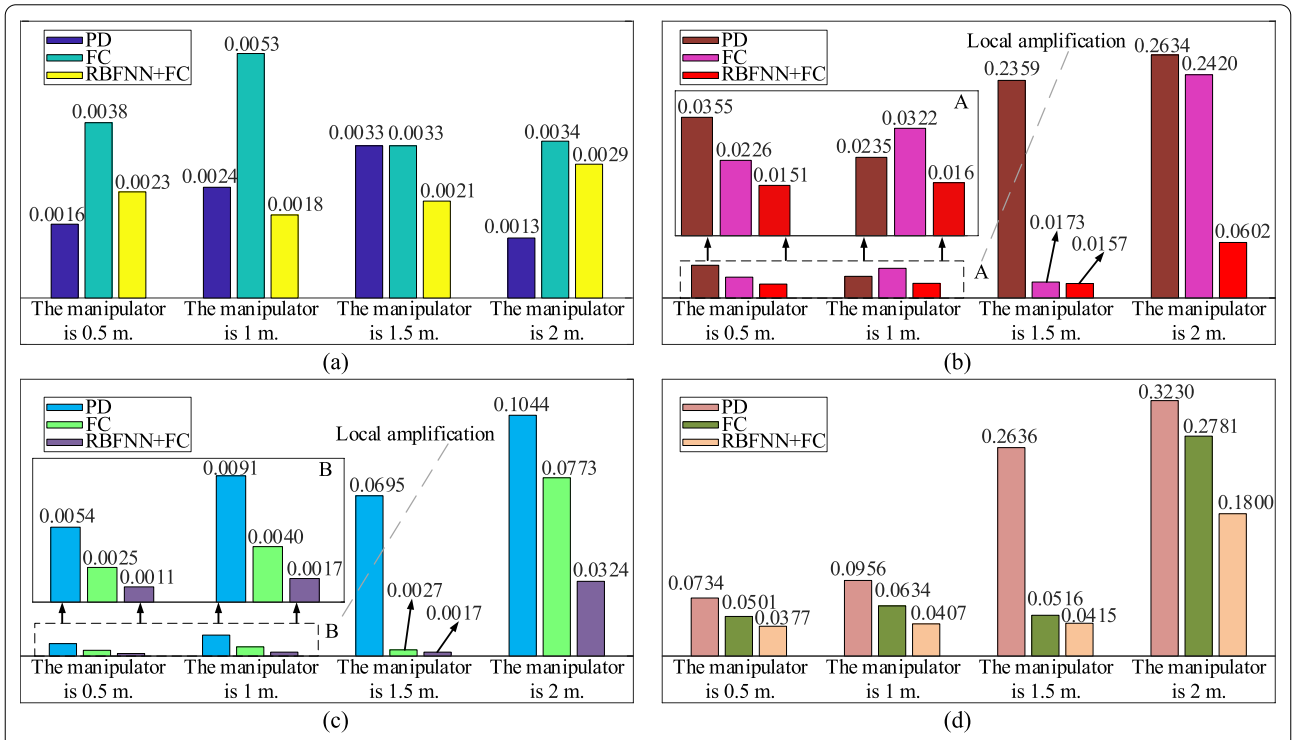

Figure 16 Histogram of error evaluation index: (**a**) Means of errors, (**b**) Means of absolute errors, (**c**) Variance of errors, (**d**) Standard deviation of errors

fuzzy control strategies gradually increase. When the flexible manipulator's length is negligible, an error can be obtained using fuzzy control. However, when the flexible manipulator's length increases, the combined control strategy can still yield a negligible error. Therefore, the combined control strategy is more suitable for flexible manipulators with larger lengths.

According to Figure 16, it can be observed that the three different control strategies have no significant effect on the means of errors. It is also impossible to measure the quality of a control strategy based on the means of errors. However, the means of absolute errors, variances, and standard deviations of the errors can represent the control accuracy of flexible manipulators. When the

flexible manipulator's length is long, the error evaluation indices of the feedforward PD control and fuzzy control strategies become poor. However, the error evaluation index using the combined control strategy exhibits negligible change. This is consistent with the conclusions obtained from the simulations. This indicates that the combined control strategy can effectively reduce the rotation angle error of the flexible manipulators and improve the control accuracy.

5 Conclusions

1. When flexible manipulators had long length and high speed, the flexible coupling nonlinear terms had a greater influence on the deformation and input torque of the manipulators. Therefore, the influence of nonlinear terms cannot be ignored under these working conditions.
2. The length of a telescopic flexible manipulator altered during movement, which caused the dynamic parameters to exhibit time-varying characteristics. The combination of nonlinear and time-varying parameters formed the uncertainty component of the dynamic model. The existence of the uncertain part caused difficulties in the rotation angle control of flexible manipulators. The feedforward PD and fuzzy control strategies achieved accurate control when the length of the flexible manipulator was short. However, with an increase in the length of the manipulator, control strategies gradually became ineffective.
3. With the combined control strategy, accurate rotation angle control was achieved when the length of the manipulator increased. Compared with feedforward PD and fuzzy controls, the combined control effectively reduced the variances and standard deviations of the errors. When the flexible manipulator was long, the error variances in the combined control strategy were reduced by 65%. The standard deviations of the errors decreased by 43%. Therefore, it was demonstrated that the combined control strategy is more suitable for telescopic flexible manipulators.

Acknowledgements
The authors thank the *Shenyang Institute of Automation, Chinese Academy of Sciences*, for their help with the control experiments. We are especially grateful to Prof. Zhigang Xu for his support and assistance with the control experiment of the flexible manipulator.

Authors' Information
Dongyang Shang, born in 1995, is currently a Ph.D. candidate at the *School of Mechanical Engineering and Automation*, *Northeastern University*, *China*. He received his bachelor's degree from the *Shenyang Aerospace University, China*, in 2018. His research interests include control theory, applications, and manipulator control with flexible joints.
Xiaopeng Li, born in 1976, is currently a professor at the *School of Mechanical Engineering and Automation*, *Northeastern University, China*. He received his Ph.D. from the *Northeastern University*, *China,* in 2006. He specializes in machine design theory and methodology, mechanical dynamics, and friction-induced vibrations. He is the Assistant Director of the *Institute of Mechanical Design and Theory, Northeastern University, China*.
Meng Yin received his Ph.D. from the *State Key Laboratory of Robotics, Chinese Academy of Sciences, University of Chinese Academy of Sciences, China*. He is currently a post-doctoral researcher at the *Shenzhen Institute of Advanced Technology*, *Chinese Academy of Sciences, Shenzhen, China*. His research interests include tendon sheath-driven humanoid robots, medical robots, and industrial automation.
Fanjie Li, born in 1994, is currently a Ph.D. candidate at the *College of Mechanical Engineering and Automation, Northeastern University, China*. He received his bachelor's degree from *Yantai University, China,* in 2017. His research interests include vehicle suspension systems and transmission-line inspection robots.
Bangchun Wen, born in 1930, is currently a professor at the *School of Mechanical Engineering and Automation, Northeastern University, China*. He was elected an academician at the *Chinese Academy of Sciences* in 1991. He is currently a member of the *International Rotor Dynamics Technical Committee and of the China Committee of the International Federation of Machine Theory and Institutions*. He has been engaged in the teaching of mechanical and vibration engineering for a long time and has made important contributions to the training of various types of students.

Author contributions
DS wrote the manuscript; XL and MY were in charge of the whole trial; and FL and BW assisted with sampling and laboratory analyses. All authors have read and approved the final manuscript.

Funding
Supported by National Natural Science Foundation of China (Grant No. 51875092), National Key Research and Development Project of China (Grant No. 2020YFB2007802), Natural Science Foundation of Ningxia Province (Grant No. 2020AAC03279), and Fundamental Research Funds for the Central Universities (Grant No. N2103025).

Competing interests
The authors declare no competing financial interests.

Author Details
[1]School of Mechanical Engineering and Automation, Northeastern University, Shenyang 110819, China. [2]Shenzhen Institutes of Advanced Technology, Chinese Academy of Sciences, Shenzhen 518055, China.

Received: 20 April 2021 Revised: 21 March 2022 Accepted: 8 April 2022
Published online: 20 May 2022

References

[1] Q L Hu, G F Ma. Variable structure control and active vibration suppression of flexible spacecraft during attitude maneuver. *Aerospace Science and Technology*, 2005, 9(4): 307-317.
[2] M H Korayem, S F Dehkordi. Dynamic modeling of flexible cooperative mobile manipulator with revolute-prismatic joints for the purpose of moving common object with closed kinematic chain using the recursive Gibbs–Appell formulation. *Mechanism and Machine Theory*, 2019, 137: 54-279.
[3] Y Yamamoto, X P Yun. Effect of the dynamic interaction on coordinated control of mobile manipulators. *IEEE Transactions on Robotics & Automation*, 1996, 12(5): 816-824.
[4] Z J Li, J G Gu, A G Ming, et al. Intelligent compliant force/motion control of nonholonomic mobile manipulator working on the nonrigid surface. *Neural Computing & Applications*, 2006, 15(3): 204-216.
[5] D W Wei, T Gao, X J Mo, et al. Flexible bio-tensegrity manipulator with multi-degree of freedom and variable structure. *Chinese Journal of Mechanical Engineering*, 2020, 33: 3.
[6] W He, T T Wang, X Y He, et al. Dynamical modeling and boundary vibration control of a rigid-flexible wing system. *IEEE/ASME Transactions on Mechatronics*, 2020, 25(6): 2711-2721.

[7] M A Eshag, L Ma, Y Sun, et al. Robust boundary vibration control of uncertain flexible robot manipulator with spatiotemporally-varying disturbance and boundary disturbance. *International Journal of Control Automation and Systems*, 2021, 19(2): 788-798.
[8] H B Yin, Y Kobayashi, J L Xu, et al. Theoretical and experimental investigation on decomposed dynamic control for a flexible manipulator based on nonlinearity. *Journal of Vibration and Control*, 2014, 20(11): 1718-1726.
[9] A K Padthe, B Drincic, J oh, D D Rizos, et al. Duhem modeling of friction-induced hysteresis - Experimental determination of gearbox stiction. *IEEE Control Systems Magazine*, 2008, 28(5): 90-107.
[10] D Halim, X Luo, P M Trivailo. Decentralized vibration control of a multi-link flexible robotic manipulator using smart piezoelectric transducers. *Acta Astronautica*. 2014, 104(1): 186-196.
[11] K Ali, K E Ali, T Afshin. Dynamic analysis of flexible parallel robots via enhanced co-rotational and rigid finite element formulations. *Mechanism and Machine Theory*, 2019, 139: 144-173.
[12] M Q Shao, Y M Huang, V V Silberschmidt. Intelligent manipulator with flexible link and joint: modeling and vibration control. *Shock and Vibration*, 2020: 5-15.
[13] L H Wang, Z D Hu, Z Zhong, et al. Dynamic analysis of an axially translating viscoelastic beam with an arbitrarily varying length. *Acta Mechanica*, 2010, 214(3-4): 225-244.
[14] B Altiner, A Delibasi, B Erol. Modeling and control of flexible link manipulators for unmodeled dynamics effect. *Proceedings of the Institution of Mechanical Engineer Part I-Journal of Systems and Control Engineering*, 2019, 233(3): 45-263.
[15] E A Alandoli, T S Lee. A critical review of control techniques for flexible and rigid link manipulators. *Robotica*, 2020, 38(12): 2239-2265.
[16] F M Han, Y M Jia. Sliding mode boundary control for a planar two-link rigid-flexible manipulator with input disturbances. *International Journal of Control Automation and Systems*, 2020, 18(2): 351-362.
[17] J F Hu, X F Cui, P Li. Vibration suppression of flexible parallel manipulator based on sliding mode control with reaching law. *Applied Mechanics and Materials*, 2012, 160: 30-34.
[18] C Y Su, Y Stepanenko. Backstepping based hybrid adaptive control of robot manipulators incorporating actuator dynamics. *International Journal of Adaptive Control & Signal Processing*, 2015, 11(2): 141-153.
[19] H F Ho, Y K Wong, A B Rad. Robust fuzzy tracking control for robotic manipulators. *Simulation Modelling Practice & Theory*, 2007, 15(7): 801-816.
[20] Q J Yao. Adaptive fuzzy neural network control for a space manipulator in the presence of output constraints and input nonlinearities. *Advances in Space Research*, 2021, 67(6): 1830-1843.
[21] K Rsetam, Z W Cao, Z H Man. Cascaded extended state observer based sliding mode control for underactuated flexible joint robot. *IEEE Transactions on Industrial Electronics*, 2020, 67(12): 10822-10832.
[22] J Li, K F Ma, Z J Wu. Prescribed performance control for uncertain flexible-joint robotic manipulators driven by DC motors. *International Journal of Control Automation and Systems*, 2021.
[23] S Y Dian, L Chen, H Son. Dynamic balance control based on an adaptive gain-scheduled backstepping scheme for power-line inspection robots. *IEEE/CAA Journal of Automatica Sinica*, 2019, 6(1): 201-211.
[24] Y Meng, Z G Xu, Z L Zhao, et al. Mechanism and position tracking control of a robotic manipulator actuated by the tendon-sheath. *Journal of Intelligent & Robotic Systems*, 2020, 100(3-4): 849-862.
[25] Q C Wu, D W Xu, B Chen. Integral fuzzy sliding mode impedance control of an upper extremity rehabilitation robot using time delay estimation. *IEEE Access*, 2019, 7:1156513-156525.
[26] L Li, J K Liu. Neural-network-based adaptive fault-tolerant vibration control of single-link flexible manipulator. *Transactions of the Institute of Measurement & Control*, 2020, 42(3): 430-438.
[27] Q C Wu, X S Wang, B Chen. Neural network–based sliding-mode control of a tendon sheath–actuated compliant rescue manipulator. *Proceedings of the Institution of Mechanical Engineers Part I Journal of Systems and Control Engineering*, 2019, 233(8): 1055-1066.
[28] D Y Shang, X P Li, M Yin, et al. Control method of flexible manipulator servo system based on a combination of RBF neural network and pole placement strategy. *Mathematics*, 2021, 8(9): 1-28.
[29] D K Do. Inverse optimal boundary tracking control and observer design for a one-link rotating flexible arm. *Journal of Dynamic System Measurement and Control-Transactions of the ASMS*, 2020, 142(12): 1-12.
[30] A Abe. Trajectory planning for residual vibration suppression of a two-link rigid-flexible manipulator considering large deformation. *Mechanism and Machine Theory*, 2009, 44: 1627-1639.
[31] C Damaren, I Sharf. Simulation of flexible-link manipulators with inertial and geometric nonlinearities. *Journal of Dynamic System Measurement and Control-Transactions of the ASMS*, 1995, 117(1): 74-87.
[32] X P Li, D Y Shang, H Y Li, et al. Resonant suppression method based on pi control for serial manipulator servo drive system. *Science. Progress*, 2020, 103(1): 1-33.